Macromolecules

pubs.acs.org/Macromolecules Article

Flexibility, Extensibility, and Ratio of Kuhn Length to Packing Length Govern the Pinching Dynamics, Coil-Stretch Transition, and Rheology of Polymer Solutions

Jelena Dinic and Vivek Sharma*

Cite This: *Macromolecules* 2020, 53, 4821−4835 Read Online

ACCESS | Metrics & More | Article Recommendations | Supporting Information

ABSTRACT: We elucidate the influence of chemical structure on macromolecular hydrodynamics, rheological response, and pinching dynamics underlying drop formation/liquid transfer using polyethylene oxide (PEO) and 2-hydroxyethyl cellulose (HEC) as two polymers with distinct Kuhn length and matched overlap concentrations. We contrast the filament pinching dynamics and extensional rheology response using dripping-onto-substrate rheometry protocols. Even though dilute aqueous solutions of both polymers at matched concentrations display comparable shear viscosity, the PEO solutions exhibit distinctively higher values of extensional relaxation time, extent of strain hardening, and transient extensional viscosity, as well as an overall delay in pinch-off. We critically analyze the radius evolution for a pinching filament to posit that the solutions of flexible PEO macromolecules exhibit signatures of underlying coil-stretch transition manifested as a discontinuous, nonmonotonic variation in the extensional rate. In contrast, the solutions of semiflexible HEC show a monotonic increase in extensional rate in response to rising interfacial stress in the pinching filament, implying that the macromolecules undergo progressive stretching and orientation without undergoing coil-stretch transition. We show that the chemistry-dependent contrast in macromolecular dynamics and extensional rheology response can be characterized *a priori* in terms of three ratios: contour length to Kuhn length (flexibility), contour length to unperturbed coil size (extensibility), and packing length to Kuhn length (a parameter we termed as segmental dissymmetry). We identify the influence of the three ratios − flexibility, extensibility, and segmental dissymmetry − on the critical minimum concentration below which elastocapillary response and extensional relaxation time cannot be measured, the critical concentration above which the influence of concentration fluctuations disappears, and also define a stretched overlap concentration below which the extensional relaxation time becomes concentration-independent.

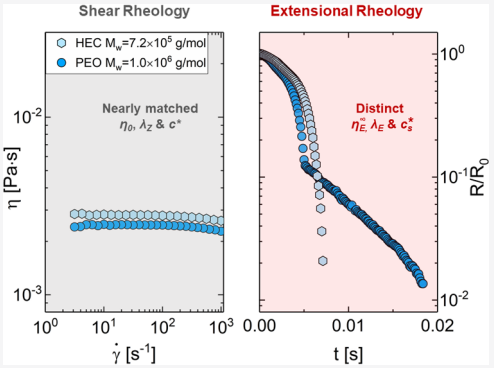

INTRODUCTION

One of the long-standing and challenging goals of macromolecular science and engineering research is to identify and elucidate how the macroscopic rheological behavior and processability depend on macromolecular parameters and interactions.[1−7] Several excellent texts[1−3] and reviews[4−9] discuss substantial progress made in identifying chemistry-independent universalities in shear rheology response of polymer solutions and melts at large lengths and long timescales. However, the influence of macromolecular parameters and interactions on the response to extensional flows remains relatively less well understood,[6−9] partially due to the challenges involved in the description of the dynamics of stretched and orientated chains[6−13] and the well-documented challenges of extensional rheometry.[8,9,13−19] In a series of recent studies,[20−25] we established dripping-onto-substrate (DoS) rheometry protocols that involve visualization and analysis of capillarity-driven pinching of liquid filaments (or necks) created by dripping a fixed volume of a fluid onto a substrate. These protocols enable the characterization of the response to extensional flow associated with stream-wise velocity gradients within pinching necks and facilitate quantitative measurement of non-Newtonian extensional rheology for complex fluids that show no signature of viscoelasticity in conventional shear and extensional rheometry.[20−26] In this contribution, we utilize DoS rheometry to characterize the pinching dynamics and extensional rheology of aqueous solutions of 2-hydroxyethyl cellulose (HEC) and polyethylene oxide (PEO) to elucidate the influence of chemical structure (i.e., polymer choice and resulting macromolecular parameters). We describe how this pursuit involves a myriad of intertwined quests and insights into fluid mechanics and nonlinear viscoelasticity, coil-stretch transition (and

Received: January 11, 2020
Revised: May 11, 2020
Published: June 8, 2020

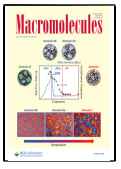

https://dx.doi.org/10.1021/acs.macromol.0c00076
Macromolecules 2020, 53, 4821−4835

hysteresis), conformation-dependent hydrodynamic and excluded volume interactions, and finite extensibility. We infer that the influence of chemistry can be evaluated *a priori* using three macromolecular parameters − flexibility, extensibility, and segmental dissymmetry − defined and detailed herein.

The contrast in local flexibility or stiffness scales with the magnitude of Kuhn length b_K or persistence length $l_p = b_K/2$ as l_p is the characteristic length scale correlated with an exponential decay in angular correlations along a chain backbone.[1−5] Polymers can be classified as globally flexible, semiflexible, or rigid rods[1,2,7,27,28] by comparing the Kuhn length b_K to the contour length, $R_{max} = N_K b_K$ or on the basis of their ratio, $N_K = R_{max}/b_K$. Biomacromolecules like DNA, actin, collagen, and polysaccharides, as well as synthetic polymers like poly(benzyl glutamate) and Kevlar, are often considered semiflexible[1,2,7,27−30] due to the relatively large values of l_p. Semiflexibility influences both thermodynamic and hydrodynamic properties.[1−3,7,27−33] Here, we consider polysaccharides to be semiflexible chains, recognizing the fact that their static and dynamic behavior is distinct from the behavior exhibited by semiflexible filaments like actin, collagen, carbon nanotubes, and fd-virus; for the latter, the contour length is comparable to the persistence length or $N_K \approx O(10)$ (or lower).[30,34,35] In this contribution, we specifically chose HEC and PEO with comparable molecular weight and matched overlap concentration c^*. Nevertheless, the computed $N_K = 70$ for HEC ($M_w = 7.2 \times 10^5$ g/mol) is nearly two orders of magnitude lower than $N_K = 9280$ for PEO ($M_w = 1 \times 10^6$ g/mol), whereas $b_K^{HEC} = 20$ nm is relatively large in comparison to $b_K^{PEO} = 1.1$ nm. Using torsional rheometry, we verify that the concentration-dependent shear viscosity values are nearly matched for dilute solutions ($c < c^*$), as expected for solutions of polymer with comparable coil size and number density of coils.[6] However, we find that the pinching dynamics and extensional rheology response of aqueous PEO and HEC solutions exhibit chemistry-based differences not anticipated by theoretical studies, including the Entov−Hinch model[36] and its variants discussed in papers since.[17,37−41]

Three regimes with distinct kinematics are anticipated in the radius evolution of capillarity-driven pinching (a terse and apt alternative to the phrase "capillary-driven thinning and breakup") of the viscoelastic fluid filament:[17,37−41] (I) a Newtonian regime, with radius evolution captured by inertiocapillary (IC) response with $R(t) \propto ((t_p - t)/t_{IC})^{2/3}$ or viscocapillary (VC) response with $R(t) \propto (t_p - t)/t_{VC}$, if the Ohnesorge number $Oh = t_{VC}/t_{IC} > 1$ (here, $Oh = \eta/\sqrt{\rho\sigma R_0}$ represents a dimensionless viscosity for a fluid with viscosity η and surface tension σ and t_p refers to the pinch-off time); (II) an elastocapillary (EC) regime, with exponential decay in the filament radius $R(t) \propto \exp(-t/\lambda_{EC})$ that allows the computation of relaxation time λ_{EC}; and (III) a terminal viscoelastocapillary (TVEC) response with $R(t) \propto (t_f - t)/t_{TVEC}$ that arises due to finite extensibility effects[22,36−38,42] and yields measurements of the steady, terminal extensional viscosity η_E^∞ (where $t_{TVEC}/t_{VC} = \eta_E^\infty/3\eta$) and the filament lifespan t_f (or the overall pinch-off time). Extensional viscosity of FENE-P chains (finitely extensible nonlinear elastic, with Peterlin's pre-averaging approximation) in ultradilute solutions can be written as $\eta_E^\infty \to 3\eta_s + 2\eta_p L_E^2$, exhibiting a dependence on both polymer contribution to shear viscosity η_p and the finite extensibility parameter $L_E^2 = (R_{max}/R_{us})^2 = N_K^{2(1-\nu)}$, defined as the ratio of the contour length of a chain $R_{max} = N_K b_K$ to the unstretched length $R_{us} = \langle R_0 \rangle^{1/2} = N_K^\nu b_K$. Thus, in addition to N_K, the finite extensibility parameter depends on the polymer−solvent interactions (including the excluded volume interactions)[17] that determine the value of the solvent quality exponent ν.

The value of $L_E^2 = 3720$ computed for the flexible PEO ($M_w = 1 \times 10^6$ Da) is significantly greater than $L_E^2 = 46$ obtained for the semiflexible HEC of a comparable molecular weight ($M_w = 7.2 \times 10^5$ Da). Thus, dilute solutions of HEC and PEO with nearly matched measured shear viscosity and (estimated) relaxation time are expected to show matched response in the Newtonian and EC regimes based on the Entov−Hinch model (and its variants),[17,37−41] with a contrast in the pinching dynamics anticipated only in the TVEC regime due to distinct values of L_E^2 and η_E^∞. Such close, quantitative comparisons have not been made in the literature, and we show that these expectations are not realized in practice. The lack of such data and comparisons is partially due to the challenges involved in the characterization of capillarity-driven pinching of a filament created by applying step strain to a fluid confined between two plates,[17,18,37,38,43−49] likewise in the commercially available technique called CaBER (capillary breakup extensional rheometer). Four significant issues arise: (i) Pinch-off occurs before plate separation even with rapid step strain for low-viscosity (η<50 mPa·s) or low-elasticity (λ<1ms) fluids.[18] (ii) The IC/VC-EC transition is not visualized (or gets masked) for unentangled polymer solutions,[22,39] and the EC regime for the semidilute solutions is neither easy to define nor to fit.[50] (iii) The TVEC (or finite extensibility) regime and EC-TVEC transition are typically not captured.[22] (iv) The extensional relaxation time $\lambda_E = \lambda_{EC} > \lambda_s$ obtained from the EC fit is greater in magnitude and exhibits stronger concentration dependence than the longest shear relaxation time λ_s for unentangled flexible polymer solutions like PEO.[39,49] We have established that the dripping-onto-substrate (DoS) rheometry protocols help overcome the first three characterization challenges,[20−25] whereas understanding the origin of concentration-dependent variation in the extensional rheology response requires a careful assessment of stretched polymer physics.[6−11,19−24,51−56] A companion paper to the current work focuses on the specific challenges that arise for HEC solutions due to extremely short-lived EC and TVEC regimes in both unentangled and entangled solutions[26] and the manifestation of an additional power law regime modulated by viscoelasticity in the filament radius evolution data for entangled HEC solutions.

Clasen *et al.*[39] attributed the higher extensional relaxation time values ($\lambda_E > \lambda_s$) in dilute polymer solutions to an increased overlap of chains stretched by strong extensional flows and mentioned the possibility of coil-stretch transition. In 1970s, deGennes,[3,55] Tanner,[57] and Hinch[56] discussed that chains undergo coil-stretch transition beyond a critical extension rate, $\dot{\varepsilon}_{c\to s}$, and due to coil-stretch hysteresis, the prestretched chains relax back by undergoing stretch-coil transition $\dot{\varepsilon}_{s\to c} < \dot{\varepsilon}_{c\to s}$ at a lower rate, implying that the stretched state of polymers can be maintained if the deformation rate stays above $\dot{\varepsilon}_{s\to c}$. The physical reality of coil-stretch hysteresis remained under scrutiny[56−59] until DNA-based microfluidics experiments by Schroeder *et al.*[60,61] showed both transition and hysteresis. Furthermore, simulations by Schroeder *et al.*[60,61] and by Hsieh and Larson[62−64] demonstrated that coil-stretch hysteresis manifests itself if $\zeta_s/\zeta_c > 4.5$ or the ratio of drag coefficients of stretched to unperturbed coils exceeds a critical value of 4.5. The drag ratio itself depends on two ratios: the extensibility L_E

https://dx.doi.org/10.1021/acs.macromol.0c00076
Macromolecules 2020, 53, 4821−4835

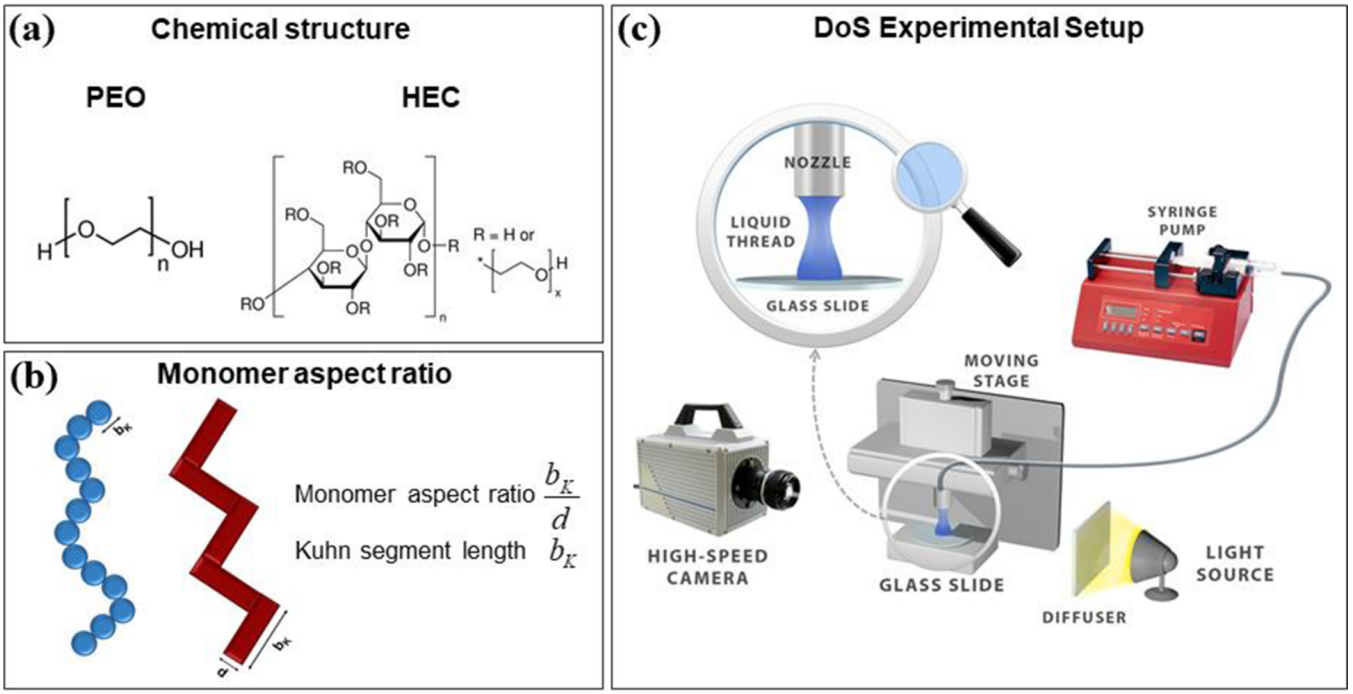

Figure 1. Chemical structure of PEO and HEC polymers, schematics showing polymers with contrast in monomer aspect ratio, and a schematic of the dripping-onto-substrate (DoS) rheometry. (a) Chemical structures of PEO and HEC. (b) Semiflexible polymers (red) show a larger aspect ratio, defined as the ratio of the Kuhn length b_K to the diameter of a Kuhn segment, d. (c) Schematic for the DoS rheometry setup shows an imaging system that consists of a high-speed camera (Fastcam SA3 with magnification optics comprising of a train of lenses including Nikkor 3.1× zoom (18−25 mm) lens and a macro lens) and a light source with a diffuser. Also shown is a dispensing system that consists of a syringe pump connected to a nozzle with outer diameter $D_0 = 2R_0 = 1.27$ mm and inner diameter $D_i = 0.838$ mm for releasing finite fluid volume onto a substrate to create an unstable liquid bridge with a filament that undergoes capillarity-driven pinching (highlighted in the inset within the schematic).

and the aspect ratio b_K/d determined by the hydrodynamic diameter of the Kuhn segment d that could differ from the actual diameter d_K and from an effective diameter (with excluded volume and other interactions included). However, as b_K/d is not easily measured or computed, we introduce a related ratio that we call segmental dissymmetry, $S_d = b_K/p$, by postulating that the criteria for coil-stretch transition and hysteresis can be rewritten in terms of packing length p. Fetters *et al.*[65−68] have shown that for flexible polymers like PEO, the plateau modulus G_e, entanglement molecular weight M_e, and tube length a can all be defined in terms of a packing length that was identified by Witten *et al.*[69] as a length scale that provides a measure of polymer elasticity. Most significantly, we postulate and argue that the same set of three macromolecular parameters − flexibility, extensibility, and segmental dissymmetry − enables us to distill the influence of chemical structure on macromolecular dynamics and viscoelastic effects associated with coil-stretch transition and hysteresis[7,8,60,61,63] as well as entanglements[65−67] and, consequently, on the shear and extensional rheological response, capillarity-driven pinching dynamics, and processability.

MATERIALS AND METHODS

The semiflexible HEC is a nonionic cellulose ether produced by etherification reaction of cellulose with ethylene oxide, whereas PEO is a flexible, nonionic water-soluble polymer. The HEC repeat unit is bulkier and has larger side groups compared to the corresponding unit of poly(ethylene oxide), leading to a larger and more asymmetric Kuhn segment due to steric hindrance and bond angle restrictions, as summarized in Figure 1. Aqueous solutions of HEC (Sigma-Aldrich; $M_w = 7.2 \times 10^5$ g/mol; degree of substitution, 2.5) and aqueous solutions of PEO (Sigma-Aldrich; $M_w = 1.0 \times 10^6$ g/mol) were prepared by slowly adding the polymer, in its as-received powder form, to deionized water. The polymer concentrations of the prepared aqueous HEC and PEO solutions were below $c = 2.0$ wt % (and for PEO, as low as $c = 0.001$ wt %). After careful addition of the polymers, solutions were placed on a roller for several days to achieve homogeneous mixing. Mixers that impose a high deformation rate are usually avoided for preparing polymer solutions as these are known to cause chain scission.[70−72] The shear rheology response of the polymer solutions was characterized using a concentric cylinder (double gap) Couette cell for low-viscosity aqueous HEC and PEO solutions (η_0<0.2 Pa·s) and cone-and-plate geometry (50 mm diameter, 1° cone) for higher-viscosity solutions on an Anton Paar MCR 302 rheometer (torque range, 10^{-5} to 200 mN·m) at 25 °C. The steady shear viscosity $\eta(\dot{\gamma}) \equiv \tau/\dot{\gamma}$ was computed from the measured shear stress τ resulting from a specified applied shear rate, $\dot{\gamma} = 10^0 - 10^3$ s^{-1}.

Characterization of capillarity-driven pinching dynamics and extensional rheology response was carried out using dripping-onto-substrate (DoS) rheometry, as shown schematically in Figure 1c. The DoS rheometry protocols rely on high-speed visualization and analysis of the radius evolution of a pinching filament (or thinning fluid neck) formed by releasing a finite fluid volume from a nozzle onto a partially wetting substrate, placed at constant height H such that $H/D_0 \approx 3$. Several papers, including our previous contributions,[20−26,73,74] can be consulted for detailed account of the utility and application of DoS rheometry protocols for measurements of capillarity-driven pinching dynamics and extensional rheology response for a range of complex fluids, including polymer and polyelectrolyte solutions,[20−26,73−78] inks,[21,79] micellar solutions,[21,80−82] and yield stress fluids[21] including particle suspensions, Carbopol solutions, emulsions, foods (mayonnaise and ketchup), and cosmetics.[21] The DoS videos obtained at a high frame rate (8000−20,000 fps or frames per second) were analyzed using ImageJ[83] and MATLAB using specially written codes for edge detection and for determination of pinching filament radius as a function of time (codes and procedure are outlined in the Supporting Information).

https://dx.doi.org/10.1021/acs.macromol.0c00076
Macromolecules 2020, 53, 4821−4835

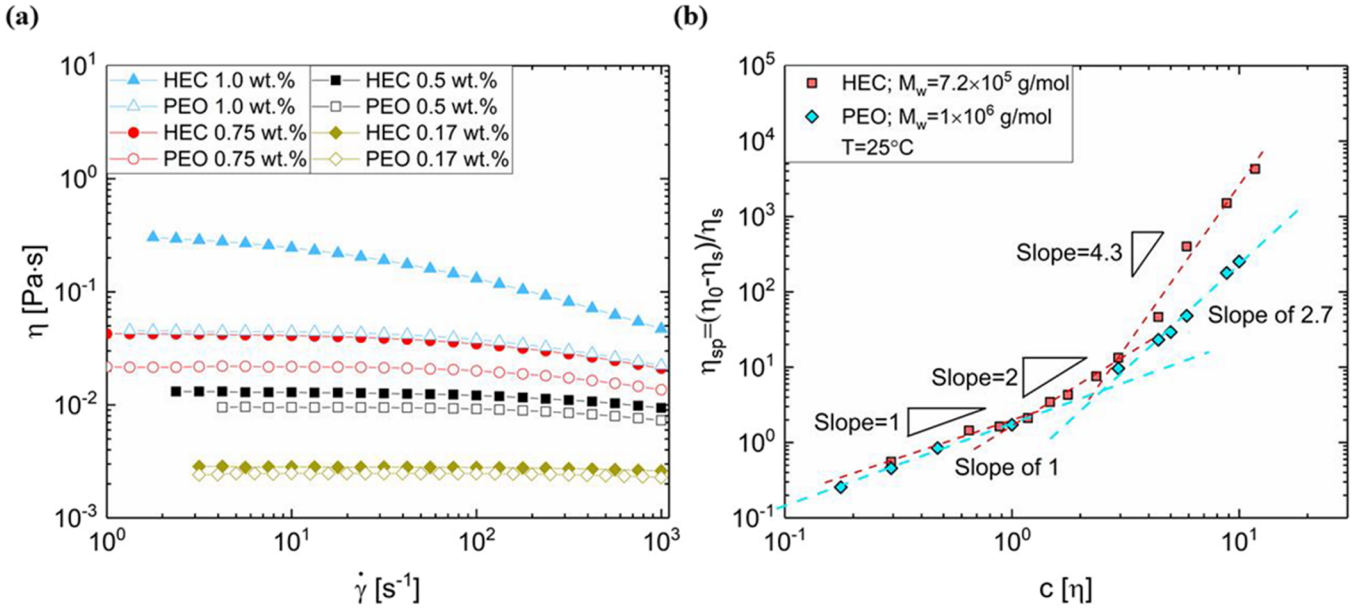

Figure 2. Shear rheology of the aqueous HEC and PEO solutions. (a) Steady shear viscosity measurements for aqueous HEC solutions are contrasted against the measured response of aqueous PEO solutions. The comparison reveals both stronger concentration-dependent increase in viscosity and higher extent of shear thinning for the HEC solutions. (b) Specific viscosity data as a function of concentration show three distinct regimes for the HEC solutions (i) dilute below overlap concentration c^* = 0.17 wt %, (ii) semidilute and unentangled ($c^* < c < c_e$), and (iii) semidilute and entangled above entanglement concentration c_e > 0.5 wt %. In contrast, for the aqueous PEO solutions, the observed behavior can be classified as dilute below c^* = 0.17 wt % and semidilute and unentangled for all PEO concentrations with $c > c^*$.

RESULTS

Contrasting Steady Shear Viscosity Measurements for Aqueous HEC and PEO Solutions. Shear viscosity measurements, as a function of shear rate obtained for a range of concentrations of aqueous solutions of HEC and PEO using a torsional rheometer, are shown in Figure 2a. A concentration-dependent increase in viscosity can be observed for both polymers. However, the zero-shear viscosity η_0 values show a stronger increase for HEC than for PEO solutions, even though η_0 values are comparable at matched concentrations below c = 0.17 wt %. Figure 2b contrasts the polymer contribution to solution viscosity in terms of computed specific viscosity $\eta_{sp} = (\eta_0 - \eta_s)/\eta_s$. At the critical overlap concentration, $c^* \approx$ 0.17 wt %, η_{sp} = 1 and the solution viscosity is twice the solvent viscosity (η_s = 0.9 mPa·s). Both overlap concentration and intrinsic viscosity ($[\eta] = 1/c^* = 5.98$ dL/g) obtained for the aqueous HEC solutions match the values obtained for the aqueous PEO solutions, implying that at matched concentrations, both polymeric systems utilized in this study exhibit matched values of overlap parameter c/c^* or Berry number $c[\eta]$. Therefore, dilute solutions of both polymers that have matched value of c/c^* or $c[\eta]$ appear indistinguishable in shear, as shown in Figure 2a. Although the nondilute solutions ($c[\eta]>1$) of both HEC and PEO exhibit shear thinning, the HEC solutions show higher zero-shear viscosity values and higher degree of shear thinning and exhibit a stronger concentration-dependent increase in specific viscosity at matched $c[\eta]$ values.

The specific viscosity of HEC solutions exhibits three distinct scaling regimes: $\eta_{sp} \propto c$ in the dilute ($c<c^*$) regime, $\eta_{sp} \propto c^2$ in the semidilute, unentangled ($c^*<c<c_e$) regime, and $\eta_{sp} \propto c^{4.3}$ in the entangled ($c>c_e$) regime. The scaling exponent in the semidilute, entangled regime (4.3, as $\eta_{sp} \approx c^{4.3}$) agrees well with the value $\eta_{sp} \approx c^{4.2}$ for $c>c_e$ reported by Del Giudice *et al.*[84] In contrast, the specific viscosity data for aqueous PEO solutions (see Figure 2b) exhibit only two regimes: $\eta_{sp} \propto c$ ($c<c^*$) and $\eta_{sp} \propto c^{2.7}$ for semidilute, unentangled ($c^*<c<c_e$) solutions. The entangled regime for flexible polymers[1] typically lies beyond $c_e/c^* \approx$ 5−10 and is beyond the range for PEO concentrations investigated herein. In contrast, for aqueous HEC solutions, the entangled regime with a stronger concentration dependence emerges beyond c_e = 0.5 wt % (corresponds to $c_e/c^* \approx$ 3), as shown in Figure 2b.

Contrasting Radius Evolution Data for Unentangled HEC and PEO Solutions. Even though the shear viscosities measured for matched dilute concentrations of PEO and HEC are quite similar, neck shape and filament radius evolution characterized using DoS rheometry protocols (see Figure 3a,b) exhibit contrasting behavior. The radius evolution for pure water (c/c^* = 0, shown as a dash-dotted blue line) exhibits characteristic inertiocapillary (IC) pinching behavior.[17,85−89] The two dilute PEO solutions at c = 0.05 wt % (blue circles, dilute regime, $c[\eta] = c/c^* \approx 0.3$) and c = 0.17 wt % (gold diamonds at an overlap concentration with $c/c^* \approx 1$), respectively, also display an initial IC regime, followed by a distinct transition to an elastocapillary (EC) regime. The EC regime appears linear in a semilog plot of filament radius vs time, as shown in Figure 3b, and the radius evolution is quantitatively described by an exponential decay of the following form

$$\frac{R(t)}{R_0} \approx \left(\frac{G_E R_0}{2\sigma}\right)^{1/3} \exp\left(-\frac{t - t_c}{3\lambda_E}\right) \quad (1)$$

The expression differs from the most often cited Entov−Hinch expression[36] in utilizing λ_E and G_E rather than the values of the longest shear relaxation time λ_s and shear modulus G. Defining the IC/VC to EC transition at t_c and fitting the elastocapillary (EC) regime using a shifted timescale ($t - t_c$) provide more physically reasonable values for G_E.[22] Thus, the

https://dx.doi.org/10.1021/acs.macromol.0c00076
Macromolecules 2020, 53, 4821−4835

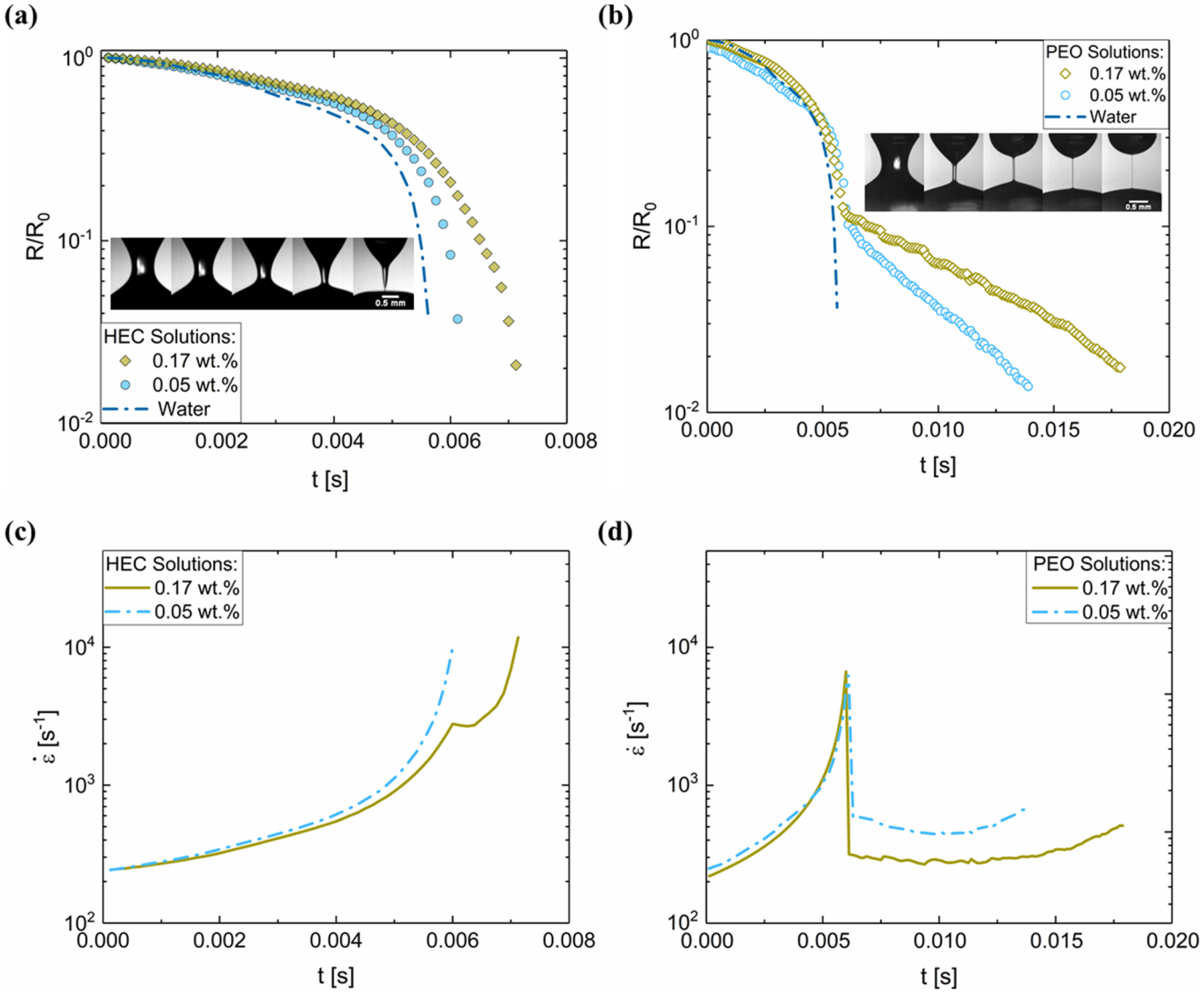

Figure 3. Contrasting the influence of the three chemistry-dependent macromolecular parameters (flexibility, extensibility, and segmental dissymmetry) on neck shape, radius evolution, and extensional rate variation with time. (a) Radius evolution datasets for two HEC solutions show a slower pinching rate and delayed pinch-off in contrast to water. The neck shape shown for 0.05 wt % HEC appears to have a pronounced cone characteristically observed during inertiocapillary pinching. (b) Radius evolution for PEO solutions shows the transition from inertiocapillary (IC) to elastocapillary (EC) pinching, and although the shear viscosity values of HEC and PEO solutions are nearly matched, the inset shows that a slender, cylindrical filament forms in the case of PEO solution. The filament lifespan t_f = 20 ms for the aqueous PEO solution is much longer than t_f = 7 ms for the aqueous HEC solution, and here, the elastocapillary span provides dominant contribution to the filament lifespan. (c) The extensional rate, determined from the filament radius evolution data, appears to increase monotonically for the HEC solutions, rising to a relatively high value of $\dot{\varepsilon} \approx 10^4\ s^{-1}$. Two regimes observed for the solution with higher concentration (c = 0.17 wt %). (d) For PEO solutions, the extensional rate exhibits a characteristic increase in the IC pinching regime and displays a sudden and precipitous drop at the onset of EC behavior. The extensional rate maintains a constant value in the EC regime but rapidly climbs again in the terminal viscoelastocapillary (TVEC) or finite extensibility regime.

prefactor in eq 1 corresponds to a critical radius $R_c \approx R_0(G_E R_0/2\sigma)^{1/3}$ determined by interplay of viscoelasticity and capillarity.[22,90] Here, the modulus obtained from the EC fit, G_E, is distinct from the relaxation modulus G obtained by fitting the relaxation spectrum data or by using $G \equiv \eta_p/\lambda_s$ such that η_p represents the polymer contribution to solution shear viscosity. Furthermore, the λ_s values cannot be otherwise measured or deduced using shear rheometry in many cases, including those for the unentangled polymer solutions in relatively low-viscosity solvents like water, as discussed here. The influence of elasticity for dilute solutions can be gauged based on the estimated value of Zimm relaxation time $\lambda_Z = \frac{1}{\zeta(3\nu)}\frac{[\eta]\eta_s M_w}{RT}$ (for a nondraining, unperturbed coil in single-chain limit). Here, the prefactor $1/\zeta(3\nu) = 1/\sum_{i=1}^{\infty}(1/i^{3\nu})$ depends on the solvent quality exponent ν. However, the estimated Zimm times only give the lowest threshold for the relaxation time as an accurate description of polymer dynamics requires accounting for both concentration-dependent and conformation-dependent hydrodynamic and excluded volume interactions.[4−11,20−24,51−55,60−64,91−94] Nevertheless, the contrast in behavior displayed at $c[\eta] = c/c^* \approx 1$ in Figure 3 is particularly remarkable as any *a priori* estimates of viscous (matched shear viscosity), elastic (comparable Zimm relaxa-

https://dx.doi.org/10.1021/acs.macromol.0c00076
Macromolecules 2020, 53, 4821−4835

tion time: λ_Z^{PEO}= 0.1 ms and λ_Z^{HEC}= 0.07 ms), and interfacial stresses (also comparable) as well as prediction for pinching dynamics in the EC regime would be similar if based on the Entov−Hinch theory or its variants that utilize either shear relaxation time or the same effective relaxation time (for both IC and EC regimes).[17,37−41,46,95,96]

At first glance, the elastocapillary response seems to be absent or imperceptible in the radius evolution plots of dilute HEC solutions. However, the neck shape before pinch-off obtained for the dilute HEC solutions is quite distinct from a single sharp cone obtained for water and other low-viscosity Newtonian fluids that undergo IC pinching. The image sequence for the HEC solution at the overlap concentration (0.17 wt %, Figure 3a) reveals that the conical neck is connected to the sessile drop by a slender cylindrical filament in the final stage before the pinch-off event. A close examination of the neck shapes for an extended range of concentrations for the aqueous HEC solutions shows that the conical neck progressively disappears in favor of a slender, cylindrical shape in nondilute solutions of HEC ($c[\eta]$>1) only after the solution shear viscosity rises to ∼10 times the solvent viscosity (detailed in a companion paper[26]). In contrast, a slender, cylindrical filament shape arises for the PEO solutions in dilute systems, even at $c[\eta]$ = 0.1, as detailed in our earlier papers.[20−23] However, the presence of a slender, cylindrical filament, delayed pinch-off (the presence of two distinct regimes for c = 0.17 wt % solution), and lack of satellite drop formation show that HEC as an additive alters the pinching dynamics, extensional rheology response, and drop size distribution.

The Tale of Two Elastocapillary Regimes. The contrast in capillarity-driven pinching dynamics and response to extensional flows are further highlighted in the plot of extensional rate vs time, as shown in Figure 3c,d. For the 0.05 wt % HEC solution, the extensional rate $\dot{\varepsilon} = -2\dot{R}/R$ computed using the radius evolution data of a pinching filament increases monotonically, whereas the rate data for the 0.17 wt % HEC solution (at $c = c^*$) appear to show a short-lived EC regime. In contrast, at matched concentrations, the extensional rate increases with time in the IC regime for the PEO solution and plunges precipitously after the IC-EC transition, exhibiting a discrete and distinctive shift to a lower rate (Figure 3d). We posit that the discrete transition in the extensional rate vs time data for PEO solutions is a signature of an underlying coil-stretch transition that occurs when the ratio of stretching rate to the relaxation rate (computed using shear relaxation time of unperturbed coils λ_s) exceeds the value of 1/2 or a critical extensional rate such that $Wi = \lambda_s\dot{\varepsilon}_{c\to s}$>1/2. The measured extensional rate in the EC regime corresponds to a low Weissenberg number, $Wi_s = \lambda_s\dot{\varepsilon}_{EC}$<0.1, if the shear relaxation time is used for the estimate. Prabhakar *et al.*[10,11] recently argued that following the coil-stretch transition, the conformation-dependent drag of flexible polymer chains leads to a coil-stretch hysteresis, allowing a lower extensional rate to be effective in preventing the already stretched chains from relaxing back. In other words, the extensional rate in the EC regime stays above the critical extensional rate at the stretch-coil transition or $\dot{\varepsilon}_{s\to c}<\dot{\varepsilon}_{EC}<\dot{\varepsilon}_{c\to s}$. The coil-stretch transition leads to a profound change in the coil conformation, which results in an effectively longer relaxation time of the stretched chains, measured or reported as extensional relaxation time λ_E. This leads to a high effective Weissenberg number, $Wi_{EC} = \lambda_E\dot{\varepsilon}_{EC} \approx 2/3$, in the EC regime. Consequently, the chains continue to experience sustained stretching in the EC regime and build-up macromolecular strain, leading to the TVEC (or the finite extensibility) regime that can be analyzed to obtain a steady, terminal extensional viscosity value that is independent of both strain and strain rate. In contrast, for HEC solutions, even though dynamics relatively close to the pinch-off event exhibit a non-Newtonian or viscoelastic response, the discrete jump or overshoot in the extensional rate, presumably associated with the changes in macromolecular dynamics after coil-stretch transition, is absent.

Several literature studies recognize that the experimentally obtained radius evolution data for flexible polymer solutions using dripping, jetting, or CaBER-like stretched liquid bridge protocols cannot be quantitatively and self-consistently modeled by numerical or analytical solutions based on Oldroyd-B, FENE-P, or Giesekus constitutive models (even if multiple modes are used).[10,11,36,46,90,97,98] Historically, Entov and Hinch[36] compared their EC expression to the experimental data reported by Liang and Macklay.[99] As the initial VC regime was not resolved in the radius evolution data obtained from stretched liquid bridges,[99] fortuitously, the comparison was carried out for t_c = 0 (see eq 1), and for nondilute solutions, their assumption of $\lambda_{EC} = \lambda_s$ is somewhat justified. Nevertheless, Entov and Hinch[36] found that including a prestretch, P in the prefactor (or using a product of G and P) was necessary to match the radius evolution profiles obtained experimentally. Subsequent studies by Anna and McKinley,[46] Tirtaatmadja *et al.*,[90] among others,[95,98] reiterate that the quantitative comparisons are unsuccessful in describing the onset (i.e., the transition point referred here in terms of R_c and t_c), duration (elastocapillary span Δt_{EC}), and decay constant (λ_{EC}, used to obtain extensional relaxation time $\lambda_E = \lambda_{EC}$) of the elastocapillary (EC) regime by use of moduli and relaxation times obtained from shear rheology measurements or theory. A few recent theoretical studies revisit the problem of capillarity-induced pinching by utilizing constitutive models that include finite extensibility but do not show coil-stretch hysteresis;[40,41,95,96] however, comparisons with experiments are not included, the possibility of coil-stretch transition (and hysteresis) is not considered, and the influence of large stretching on relaxation dynamics of stretched polymer dynamics is also not evaluated. The influence of the coil-stretch transition and hysteresis on the concentration-dependent variation of extensional relaxation time, the role of free surface flows and non-Newtonian fluid mechanics, and the influence of chemical structure are discussed in the later sections.

Filament Lifespan and Terminal Extensional Viscosity for Nondilute Solutions ($c > c^*$). At a matched degree of overlap or c/c^* value, the radius evolution data for nondilute PEO solutions ($c > c^*$) also exhibit a pronounced elastocapillary regime in contrast to the HEC solutions, as shown in Figure 4. For the PEO solutions, elastocapillary span Δt_{EC} makes the primary contribution to filament lifespan t_f. In contrast, for HEC solutions, $\Delta t_{EC} \ll t_f$ and the short Δt_{EC} results in a relatively short filament lifespan for dilute solutions as well as for the data shown in Figure 4a for semidilute solutions at $c/c^* = 3$ (even though the shear viscosity of the HEC solution is marginally higher). However, as the semiflexible HEC solutions become entangled beyond $c/c^* = 3$, the zero-shear viscosity of HEC solution at $c/c^* = 9$ (∼1.5 wt %) is nearly an order of magnitude higher than the corresponding semidilute, unentangled PEO solution at c/c^*.

https://dx.doi.org/10.1021/acs.macromol.0c00076
Macromolecules 2020, 53, 4821−4835

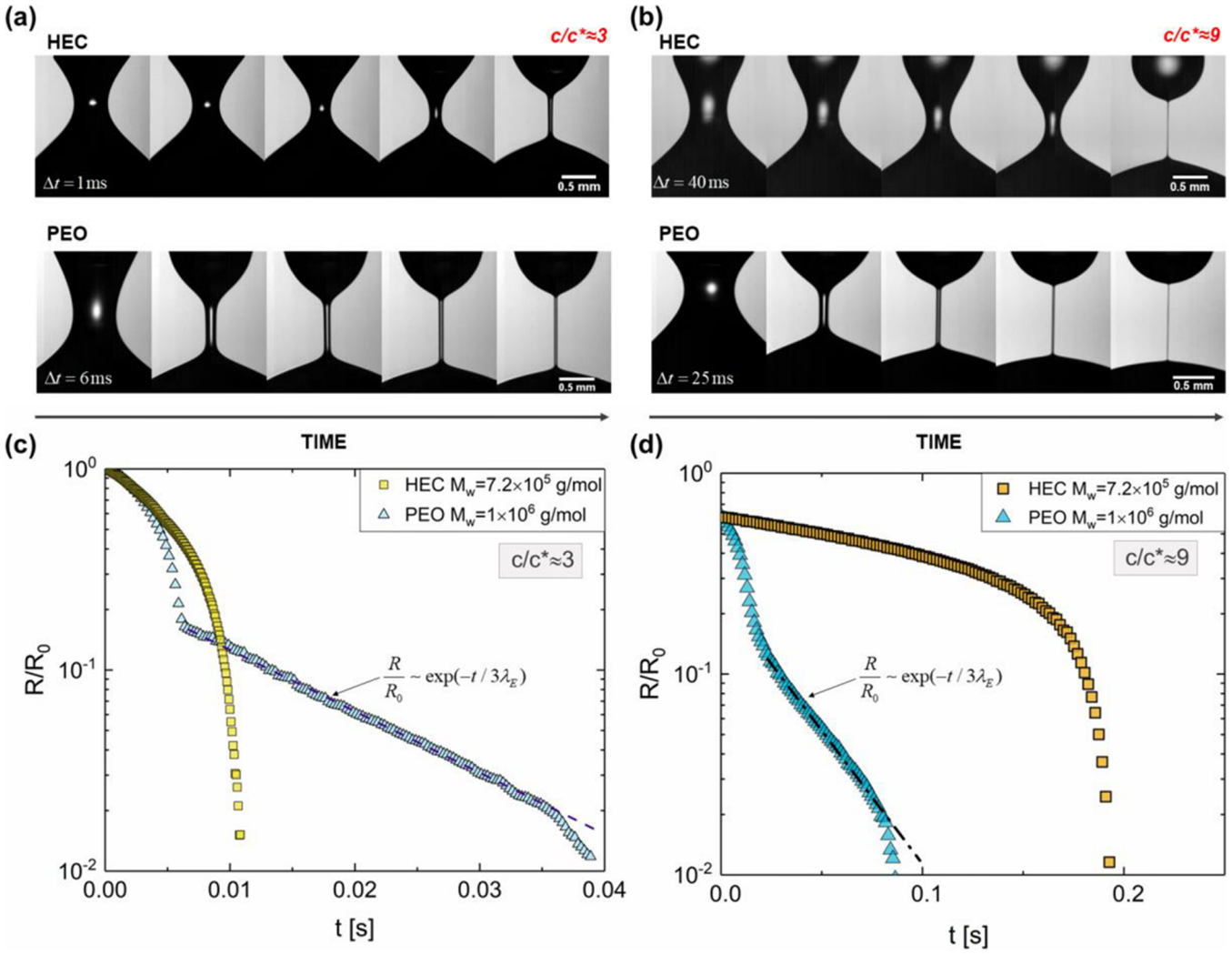

Figure 4. Comparison of the neck shape and radius evolution for nondilute aqueous PEO and HEC solutions. (a) Image sequence contrasts the neck shape and shape evolution at $c/c^* = 3$. The time elapsed between progressive snapshots is $\Delta t = 1$ ms for the HEC solution and $\Delta t = 6$ ms for the PEO solution. (b) Image sequence contrasts the neck shape and shape evolution at $c/c^* = 9$ for HEC (entangled) and PEO (unentangled) solutions. The time elapsed between progressive snapshots increases to $\Delta t = 40$ ms for the HEC solution and rises to $\Delta t = 25$ ms for the PEO solution. (c) Radius evolution in time data show striking contrast and the dashed lines represent the elastocapillary fits to PEO data using eq 1. The PEO solution thins remarkably slowly, even though the shear viscosity of the HEC solution is higher at $c/c^* = 3$. (d) Comparison of the radius evolution data for high-concentration HEC and PEO solutions ($c/c^* \approx 9$) reveals a longer filament lifespan for the HEC solution.

The relatively strong increase in shear viscosity results in substantial increases in the filament lifespan t_f for the HEC solution at $c/c^* = 9$ (~1.5 wt %) such that the t_f of the HEC solution exceeds that measured for the corresponding PEO solution, as shown in Figure 4b.

In contrast with the unentangled HEC solutions, the filament radius of the entangled HEC solutions displays the power law response, modulated by viscoelastic stresses in the last stage near pinch-off. The detailed discussion of this power law regime and the corresponding fits and analysis for HEC solutions are provided in the companion paper to this study. Radius evolution data of the nondilute solutions of both HEC and PEO solutions are fitted by both EC and TVEC regimes, yielding the values of extensional relaxation time, filament lifespan, and terminal extensional viscosity included in Table 1. Above overlap concentration, the terminal Trouton ratio $Tr^{\infty} = \eta_E^{\infty}/\eta_0$ values decrease with an increase in concentration, and we find that $Tr^{\infty} \leq 200$ obtained for the less flexible polymer (HEC) is significantly lower than $200 < Tr^{\infty} < 5000$ (see Table 1) obtained for PEO solutions at matched concentrations, implying lower extensional viscosity even if η_0 is higher for the entangled HEC solutions.

DISCUSSION

In this contribution, we argue that the contrast in the pinching dynamics and the extensional rheology response displayed by PEO and HEC of similar molecular weight has its origin in the changes in macromolecular dynamics after undergoing coil-stretch transition, first outlined theoretically in 1974 and the focus of many theoretical studies since.[6,7,11,54,55,60−64,92−94] Early experimental studies that relied on measurement of flow birefringence Δn as a function of extensional rate in stagnation point flows[13,100,101] observed coil-stretch transition as a jump at a critical extensional rate $\dot{\varepsilon}_c$ in Δn values measured for flexible polymers, in contrast with a continuous, smooth increase in Δn values with $\dot{\varepsilon}$ for semiflexible and rod-like polymers.[13,100,101] However, as measurements of flow birefringence rely on a macroscopic average of contributions

https://dx.doi.org/10.1021/acs.macromol.0c00076
Macromolecules 2020, 53, 4821−4835

Table 1. Concentration-Dependent Variation in Steady, Terminal Extensional Viscosity, Extensional Relaxation Time, and Filament Lifespan, Computed Using Radius Evolution Data for Polymer Solutions of HEC and PEO[a]

c (wt %)	η_0 (Pa·s)	η_E^∞ (Pa·s)	λ_E (s)	t_f (s)[b]
HEC, M_w = 720 kg/mol				
0.17	0.0022	0.40	2.2×10^{-4}	4×10^{-3}
0.25	0.0040	0.40	2.3×10^{-4}	4.5×10^{-3}
0.40	0.0077	0.50	2.4×10^{-4}	6.0×10^{-3}
0.50	0.013	0.90	2.9×10^{-4}	1.0×10^{-2}
0.75	0.043	1.7	4.5×10^{-4}	1.4×10^{-2}
1.0	0.36	4.0	2.5×10^{-3}	5.4×10^{-2}
1.5	1.4	7.1	1.5×10^{-2}	2.9×10^{-1}
2.0	3.8	8.5	1.2×10^{-1}	6.5×10^{-1}
PEO, M_w = 1000 kg/mol				
0.10	0.0019	7.1	1.9×10^{-3}	2.1×10^{-2}
0.20	0.0025	12	2.8×10^{-3}	3.0×10^{-2}
0.30	0.0039	18	3.3×10^{-3}	3.5×10^{-2}
0.50	0.0094	25	4.7×10^{-3}	3.7×10^{-2}
0.75	0.022	35	6.6×10^{-3}	5.3×10^{-2}
1.0	0.046	43	9.4×10^{-3}	6.9×10^{-2}
1.5	0.17	51	1.2×10^{-2}	1.0×10^{-1}
2.0	0.23	70	1.7×10^{-2}	1.8×10^{-1}

[a]Even for the solutions that have very similar zero-shear viscosity values, the response to extensional flow fields is quite distinct. [b]The value of t_f is calculated with the initial dimensionless radius value of $R/R_0 = 0.8$ for all concentrations.

by both stretching and orientation, the coil-stretch transition appeared to take place over a somewhat broad range of extensional rates. However, the single-molecule visualization experiments carried out by Schroeder *et al.*[7,8,60,61] using DNA chains provided unambiguous support for the reality of both the coil-stretch transition and coil-stretch hysteresis. Subsequently, Sridhar *et al.*[94] reported that quasi-steady state stress measurements made using a FISER (filament stretching extensional rheometer) at a narrow range of strain rates close to the coil-stress transition exhibit signatures of glasslike slowdown, and the slowing was also described theoretically.[94,102]

Most recently, Prabhakar *et al.*[10,11] argued that coil-stretch hysteresis sets the magnitude of extensional relaxation time in dilute and semidilute solutions and determined that macromolecular stretching in response to extensional flows strengthens interchain interaction for dilute solutions ($c < c^*$), causing chains to self-concentrate, in agreement with several experimental and theoretical studies.[20,22,23,39,51,90] However, as their analysis neglects the influence of excluded volume interaction and solvent quality and is limited to higher-viscosity systems that display VC-EC transition, their model does not capture the concentration-dependent variation in the extensional relaxation time for polymer solutions in good solvents (including aqueous PEO solutions[22,23,90]) or cannot capture filament radius evolution for aqueous solutions of HEC and PEO. Their model predictions[10,11] compare reasonably well with experimental results in the intrinsically semidilute solutions[20,22,39] as the influence of excluded volume interactions gets progressively screened for $c > c^*$ and the EV screening is even stronger for stretched chains in both single-chain limit[52,53] and in dilute and semidilute solutions.[9,20,22,23]

As the IC/VC-EC transition is not always resolved or observed in data obtained using CaBER experiments, the contrasting behavior shown in Figure 3 was never observed or reported as clearly in the filament radius evolution plots from CaBER. However, a stark IC-EC transition (similar to Figure 3b) and a decrease in extensional rate after transition to the EC response were experimentally observed in the filament radius evolution using dripping by Amarouchene *et al.*,[97] Tirtaatmadja *et al.*,[90] among others.[17,103,104] Amarchouene *et al.*[97] discussed the possibility of coil-stretch transition but measured a concentration-independent critical extensional rate (inversely proportional to the relaxation times) for dilute PEO solutions and reported that solutions of xanthane (M_w = 3000 kg/mol; concentrations, 25−1000 ppm) exhibit Newtonian pinching dynamics. Tirtaatmadja *et al.*[90] suggested that polymers are initially unstretched in the IC regime, and the interfacial or capillary stress is balanced by inertial acceleration in the pinching filament. After the extensional rate becomes relatively large ($Wi > 1/2$) in the rapidly pinching neck, according to Tirtaatmadja *et al.*:[90] "the polymer stretch grows rapidly in the thin filament" until "the elastic stresses grow large enough to resist the diverging capillary pressure". Tirtaatmadja *et al.*[90] plotted the overshoot in extensional rate in terms of an apparent value of Wi (assuming the same relaxation time both before and after transition). In the same contribution, Tirtaatmadja *et al.*[90] measured an increase in relaxation times with concentration but made no mention of coil-stretch transition (and hysteresis). Further research on IC-EC transition and EC response with the dripping methodology stalled, primarily due to at least two critical challenges: λ_E appears to depend on the nozzle size and drop weight, and longer-lived filaments are both difficult to visualize and prone to nonuniform stretching and bead formation.[97,103]

Even though capillary breakup extensional rheometer (CaBER) studies provide a robust alternative to dripping and more reliable characterization of the elastocapillary regime, CaBER is not suitable for the visualization of transition to the EC regime[16,18,39,47,79,99] as the low-viscosity fluids ($Oh \ll 1$, for which IC-EC transition is expected) complete pinch-off, and the high-viscosity fluids undergo VC-EC transition in many cases, even before the plate separation stage is completed. In contrast, studies using DoS rheometry protocols (including Figure 3) reveal that the sharp IC-EC transition for solutions of flexible polymers is accompanied by an overshoot in the extensional rate. But the corresponding dataset for the HEC solutions shows an absence of the sharp IC-EC transition and overshoot in the extensional rate (and, effectively, a change in chain relaxation dynamics). Pinching dynamics are markedly distinct, even though the coil size, number density of coils, viscosity, Zimm time, and surface tension are closely matched for the two polymers used in this study. The intrinsic and computed macromolecular properties/parameters, along with the respective references for the values extracted from the literature as cited or calculated using the expressions outlined in this paper, are all summarized in Table 2.

We contend that in capillarity-driven pinching, the progressive decrease in neck radius leads to a corresponding increase in the applied stress. The changes in extensional rate over time emulate, and are influenced by, the corresponding conformational changes in macromolecules. Thus, extensional rheometry protocols based on capillarity-driven pinching can be considered to be stress-controlled experiments, in contrast to the extensional rate-controlled measurements carried out by Schroeder *et al.*[7,8,60,61] and by many groups that investigated flow birefringence in stagnation point flows.[16,100,101,105] As the

https://dx.doi.org/10.1021/acs.macromol.0c00076
Macromolecules 2020, 53, 4821−4835

Table 2. Macromolecular Parameters for Aqueous PEO and HEC Molecules

parameter	polymer PEO	polymer HEC	reference
M_w (kg/mol), molecular weight (avg)	1000	720	average provided by the supplier
M_0 (g/mol), monomer molecular weight	44	272	
R_g (nm), radius of gyration	68	68	84
$\langle R_0^2 \rangle^{1/2}$ (nm), end-to-end distance	167	167	computed[9]
b_K (nm), Kuhn segment length	1.1	20–60[a]	105,106
d (nm), Kuhn segment diameter	0.5	1	computed[9]
b_K/d, Kuhn segment aspect ratio	2.2	20	computed[1]
N_K, number of Kuhn segments	9280	70	computed[107]
C_∞, characteristic ratio	6.7	21.4	108
l (nm), bond length	1.54	0.77	108
$L_c = R_{max}$ (μm), contour length	10.2	1.3	computed[107]
L_E^2, finite extensibility parameter	3720	46	computed[16]
ς_s/ς_c, drag coefficient ratio	7.8	1.4	computed[13]
$[\eta]$ (cm^3/g), intrinsic viscosity	598	598	
λ_Z (ms), Zimm relaxation time	0.1	0.07	computed[9]
λ_R (ms), Rouse relaxation time	0.14	0.09	computed[9]

[a] 20 is used in this study.

flow fields within pinching filaments emulate the real flows encountered during drop formation and liquid transfer, we suggest that an understanding of coil-stretch transition and hysteresis can be used to outline the quantitative criteria for how the choice of polymer chemistry and molecular weight influences processability, as discussed next for HEC and PEO with comparable molecular weights and similar coil size or overlap concentration. A significant contrast exists in the value of flexibility of two polymers for the local flexibility as characterized by the Kuhn segment size and the global flexibility characterized by N_K. Likewise, the extensibility L_E^2 values are nearly two orders of magnitude higher for the PEO solutions.

Is it Possible To Observe Coil-Stretch Hysteresis with Polysaccharides? The coil-stretch transition takes place beyond the critical extensional rate $Wi = \lambda_s \dot{\varepsilon}_c > 1/2$ defined by a concentration-dependent shear relaxation time. However, Schroeder *et al.*[60,61] and Hsieh and Larson[62−64] showed that coil-stretch hysteresis is manifested for DNA chains as well as synthetic polymers (such as polystyrene) if the ratio of drag coefficients of a stretched chain ς_s to a coil ς_c exceeds $\varsigma_s/\varsigma_c = 4.5$. The drag coefficient for spherical coil ς_c based on the Zimm model and ς_s for stretched chains based on the rigid rod are given as

$$\varsigma_c = (3/8)(6\pi^3)^{1/2}\eta_s R_c = 5.11\eta_s R_c \tag{2a}$$

$$\varsigma_s = \frac{6.28\eta_s R_{max}}{\ln(R_{max}/d)} = \frac{6.28\eta_s N_K b_K}{\ln(N_K b_K/d)} \tag{2b}$$

The ratio of drag coefficients of the stretched chain to the coiled chain is given by the following expression

$$\varsigma_s/\varsigma_c \approx R_{max}/R_c \ln(N_K b_K/d) \approx L_E/\ln(N_K b_K/d) \tag{3}$$

The calculation of coil-stretch transition and hysteresis criteria using the ratio of drag coefficients requires the value of an additional length scale d that represents the hydrodynamic diameter of a Kuhn segment. Even though the Kuhn length b_K values for most polymers can be obtained from experiments or theory, the values of hydrodynamic diameter d are not usually specified or measured. According to Larson,[107] the actual diameter of the Kuhn segment can be estimated using $d_K^2 l = 4M_0/0.82 j\pi N_A \rho$ by matching the volume occupied by N_K Kuhn segments of a chain with the volume per coil in a melt. The formula uses the molecular weight of a chemical monomer M_0 and bond length l and assumes that j is equal to the number of monomeric carbon atoms in the polymer backbone ($j = 2$ for polymers like PS or PE) and the factor 0.82 accounts for the tetrahedral bond angle. However, the relationship between d and d_K is not obvious.

We posit that a practically more suitable and rheologically relevant alternative for computing d is the use of packing length $p = (\pi/4)d_K^2/b_K \approx d^2/b_K$. By dividing the packing length, correlated with the entanglement modulus (the macroscopic measure of elasticity) by the Kuhn segment size (a measure of local flexibility), we obtain a new dimensionless measure we define as segmental dissymmetry

$$S_d = \frac{b_K}{p} \approx \frac{{b_K}^2}{d^2} \tag{4}$$

The segmental dissymmetry S_d values estimated using data provided by Fetters *et al.*[65−67] range from 2.5 to 4.5 for flexible polymers. The criteria for coil-stretch hysteresis can be effectively rewritten as

$$\varsigma_s/\varsigma_c \approx L_E/\ln(N_K S_d^{0.5}) \tag{5}$$

in terms of flexibility, extensibility, and segmental dissymmetry. Thus, coil-stretch transitions are most likely to occur for polymers with small segmental dissymmetry and large extensibility. Since the value of S_d is directly correlated with segmental shape and size, its value not only determines the criteria for the coil-stretch transition but also affects the propensity to form liquid crystalline phases.[2,29] In the present context for HEC molecules of M_w = 720 kg/mol in water, the ratio of drag coefficients equals 1.4, while for PEO molecules of M_w = 1000 kg/mol in water, the ratio equals 7.8. Thus, the observation of the coil-stretch transition in PEO is expected or predicted based on eq 3. To observe the coil-stretch hysteresis in unentangled HEC solutions, computation using eq 3 suggests that a molecular weight higher than 10^7 g/mol is needed. The criterion $\varsigma_s/\varsigma_c > 4.5$ was discussed first by Schroeder *et al.*[7,8,60,61] to describe their direct observations of coil-stretch transition and hysteresis of fluorescently labeled, longer bacterial genomic DNA (R_{max} = 1300 μm) with a drag ratio of 5 and the absence for λ-DNA (R_{max} = 20 μm) with a drag ratio of 1.6. In a previous study,[74] we utilized DoS rheometry to characterize the pinching dynamics and the extensional rheology response of λ-DNA. We reported that the radius evolution data display an absence of the VC-EC transition. Based on the discussion included in this contribution, the behavior exhibited by λ-DNA can be attributed to the lack of coil-stretch hysteresis.

https://dx.doi.org/10.1021/acs.macromol.0c00076
Macromolecules 2020, 53, 4821−4835

Concentration-Dependent Extensional Relaxation Times. Elastocapillary fits to the radius evolution data yield the concentration-dependent values of extensional relaxation times for both polymers, as plotted in Figure 5. The absolute value of the extensional relaxation time measured for aqueous PEO solutions at matched concentration by weight and matched Berry number is much higher. The extensional relaxation time for aqueous PEO solutions shows the two scaling exponents characteristic of dilute ($\lambda_E \propto c^{0.65}$; for $c < c^*$) and intrinsically semidilute, unentangled PEO solutions ($\lambda_E \propto c$ for $c > c^*$) previously described and determined[20,23] using DoS rheometry studies. We argued that the scaling laws arise from partial screening of excluded volume (EV) interactions in the dilute regime, whereas for $c > c^*$, the EV interactions get effectively screened at all length scales.[20] In dilute solutions, $\lambda_E \propto c^{0.65}$ was also reported by Tirtaatmadja *et al.*[90] using dripping experiments for PEO in glycerol−water mixture and using CaBER by Clasen *et al.*[39] for dilute polystyrene solutions in diethyl phthalate (in both cases, good solvents were used and data acquisition was facilitated by the use of solvents more viscous than water). However, as the HEC chains do not undergo coil-stretch transition, a weaker concentration dependence $\lambda_E \propto c^{0.32}$ associated with the Rouse−Zimm chain in a good solvent (blob model) is observed in the semidilute regime ($c^* < c < c_e$).[1] The extensional relaxation time values for the entangled HEC solutions ($c > c_e$) exhibit a strong increase with concentration $\lambda_E \propto c^{4.3}$ that mimics the exponent observed for the concentration-dependent increase in specific viscosity $\lambda_E \propto \eta_{sp} \propto c^{4.3}$.

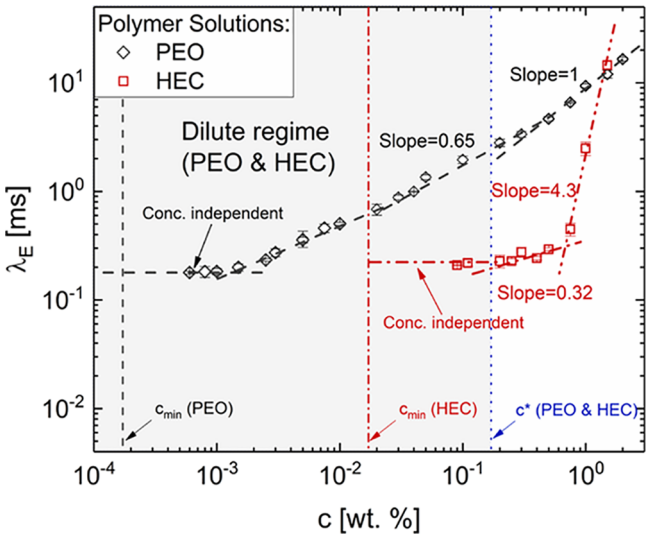

Figure 5. Concentration-dependent variations in relaxation time values for aqueous HEC and PEO solutions. (a) Extensional relaxation times for the aqueous HEC solutions are found to be lower than the values for the aqueous PEO solutions at matched concentration and matched Berry number. However, as the HEC solutions can entangle at a much lower concentration, the relaxation time shows a stronger concentration-dependent variation above $c >$ 0.5 wt %. The PEO solutions show three regimes: (i) a concentration-independent regime below c = 0.001 wt %, (ii) an extended regime with a concentration-dependent increase captured by exponent 0.65, and (iii) intrinsically semidilute solution behavior above c^*. The plot identifies a theoretical estimate for critical minimum concentration c_{min} needed for generating elastic stress that leads to the appearance of the elastocapillary regime. The existence of a concentration-independent regime is also noted.

A comparison of HEC and PEO solutions shows that the concentration-independent values of λ_E can be measured at much lower concentrations for PEO than are possible for HEC. Notwithstanding any imaging and image analysis challenges, Clasen *et al.*[39] determined that there exists a critical concentration $c_{min} = (3M_w\eta_s)/(2RT\lambda_Z L_E^2)$ below which the polymer carries less stress than a viscous solvent (even when the chains become fully stretched) and the extensional relaxation time can no longer be deduced. We can recast the formula for c_{min} using the formula for Zimm relaxation time as $c_{min}/c^* \approx 3/L_E^2$. Using Table 2, we estimate $c_{min} = 1.4 \times 10^{-4}$ wt % for PEO solutions and nearly two orders of magnitude higher concentration, $c_{min} = 1.4 \times 10^{-2}$ wt %, for HEC solutions. Thus, the calculated c_{min} concentration for HEC or PEO is only 6.4 times lower than the lowest concentration plotted in Figure 5.

Segmental Dissymmetry and Stretched Overlap Concentration. By identifying the central role of S_d (segmental dissymmetry), defined in terms of packing length p in determining coil-stretch hysteresis, we make a formal connection between the macromolecular parameters needed to describe the stretched chain hydrodynamics in dilute solutions with the chain dynamics in entangled solutions and melts. The value of S_d can be determined from rheological measurements and empirical correlations established in the literature for entangled polymers.[65−69,109] For example, the number of entanglement strands P_e in the volume equal to the cube of tube diameter (or $a = N_e^{1/2}b_K$) is given by $P_e = a/p$. For flexible polymers, a seemingly chemistry-independent constant value of $P_e \approx 20$ is observed. Thus, the S_d value can be computed to be $S_d = P_e/N_e^{1/2} \approx 20/N_e^{1/2}$ for flexible polymers, showing a direct connection of segmental dissymmetry with the entanglement molecular weight M_e. The entanglement molecular weights of polysaccharides are hard to measure as polysaccharide melts cannot be prepared, and usually, the plateau moduli of entangled polysaccharide solutions are difficult to measure reliably. However, recently, Horinaka *et al.*[110,111] computed the M_e and P_e values for several polysaccharides by utilizing rheological measurements in ionic liquids and determined P_e of 40 for amylose, 72 for carboxymethylcellulose (CMC), and 220 for cellulose. We hereby conjecture that the contrast between flexible and semiflexible polymers observed in terms of entanglement concentration (or the response to shear flow), pinching dynamics, the values of P_e, and the response to an extensional flow field appears to be correlated with the relatively high segmental dissymmetry of polysaccharides.

The experimentally determined value of HEC concentration at which the topological entanglements begin to exist in the polymer solution was found to be $c \approx 0.5$ wt % or at $c_e/c^* \approx 3$. It is well known that semidilute solutions have large concentration fluctuations, and above a critical c^{**}, the polymer solution behavior can be described using a mean field theory for concentrated solutions. Since the value of $c^{**}/c^* \approx N_K^{3\nu-1}(d^2/b_K^2)^{3\nu-1}$ depends on the Kuhn segment shape and size (assuming excluded volume value for athermal limit $b_K^2 d$ to get an upper limit), we can rewrite the expression in terms of segmental dissymmetry as $c^{**}/c^* \approx (N_K/S_d)^{3\nu-1}$. Evidently, the lower absolute values of c^{**} (and possibly, entanglement concentration) are a result of both fewer Kuhn segments and larger segmental dissymmetry for polysaccharides. More recently, Dorfman and co-workers[28] determined

https://dx.doi.org/10.1021/acs.macromol.0c00076
Macromolecules 2020, 53, 4821−4835

how the effective excluded volume parameter (or the solvent quality exponent) itself depends on the number of Kuhn segments and ratio of Kuhn segment length to diameter and thus effectively on S_d.

The extensional relaxation time data for both HEC and PEO solutions exhibit a nearly constant value below a material-dependent concentration value we named as stretched overlap concentration c_s^*, highlighting that for stretched chains, the interchain contacts are present even if the solution is considered nominally dilute on basis of the c^* value computed using the unperturbed coil size. We postulate that the stretched overlap concentration c_s^* can be estimated using theory for semidilute solutions for rod-like polymers. According to Doi and Edwards,[2] the semidilute regime for rod-like polymers spans a range between (a) the concentration at which the average distance between polymers $\vartheta^{-1/3}$ is less than the rod length or $\vartheta_1 R_s^3 < 1$ and (b) the concentration $\vartheta_2 d R_s^2 < 1$ such that the dynamic properties of finite-diameter rods are influenced by the constraint upon crossing each other. The experimental results and theoretical arguments suggest that the elastocapillary regime arises long before the coils get fully stretched. We utilize the second expression to obtain an overlap concentration for stretched chains as $c_s^*/c^* \approx 4R_g^3/dR_s^2$ or $c_s^*/c^* \approx N_K^{\nu} S_d^{1/2}/L_E^2 = N_K S_d^{1/2}/L_E^3$. The estimated value of $c_s^*/c^* \approx 0.006$ for PEO solutions is within a factor of 2 of the experimentally observed value. Likewise, Figure 5 data show that the estimated value $c_s^*/c^* \approx 0.3$ for the HEC solutions is quite close to the experimentally observed value of both stretched and standard overlap concentrations.

CONCLUSIONS

A comparison of shear and extensional rheology responses of the aqueous solutions of a semiflexible polysaccharide, hydroxyethyl cellulose (HEC), against the aqueous solutions of flexible poly(ethylene oxide) (PEO) is carried out such that the equilibrium coil size and overlap concentration (or intrinsic viscosity) are nearly matched. Hence, a matched concentration by weight corresponds to a matched value of Berry number. As expected, the steady shear viscosity of both polymers is comparable at matched concentrations in the dilute regime. The steady shear viscosity of nondilute HEC solutions was found to be higher than the viscosity of PEO solutions as HEC solutions cross over into the entangled regime at a lower concentration than PEO solutions. Aqueous solutions of both polymers show a concentration-dependent increase in extensional relaxation time and filament lifespan (or pinch-off time). Even though the shear viscosity values are matched for the dilute solutions, the PEO solutions exhibit a longer filament lifespan and higher values of both extensional relaxation time and extensional viscosity. At all concentrations, the PEO solutions exhibit higher values of the terminal extensional viscosity, even though the shear viscosity of nondilute HEC solutions ($c > c^*$) is much higher than the PEO solutions at matched concentrations (and c/c^* values). The nondilute HEC solutions exhibit a pronounced shear-thinning behavior and, for industrially relevant concentrations (typical $c < 1$ wt %), also exhibit a shorter filament timespan than the PEO solutions. Both attributes make HEC advantageous as a rheology modifier for dispensing applications: at low deformations, the dispersion behaves like a high-viscosity fluid and does not "run" or spread (helps in controlling sagging in paints), whereas at higher rates encountered during pumping or dispensing, the dispersion flows relatively easily. Furthermore, the significantly faster pinching rate and shorter filament lifespan of the unentangled HEC solutions than the unentangled PEO solutions (compared here at matched concentration for matched unperturbed coil size) make polysaccharides preferred candidates as rheology modifiers for spraying, printing, and painting applications.

Aqueous PEO solutions display a very pronounced transition from an inertiocapillary regime to a long elastocapillary regime in radius evolution of the pinching filament for dilute and some semidilute solutions (for dimensionless concentration values up to $c/c^* = 5$). We argue that the transition is associated with a discrete change in the extensional rate to a lower value, associated with the changes in macromolecular dynamics after undergoing coil-stretch transition. In contrast, the radius evolution data of the pinching filament of the aqueous solutions of semiflexible HEC display only a weak, relatively short-lived elastocapillary tail, and the extensional rate displays a nearly monotonic increase with time as the pinch-off event approaches, implying the absence of coil-stretch transition in this case. In this study, we rewrite the ratio of Kuhn segment length to diameter in terms of a ratio we call segmental dissymmetry S_d, defined using the ratio of Kuhn length to packing length p. Even if the coil-size, dilute solution rheology or values of Zimm relaxation time are matched, the coil-stretch transitions are most likely to occur for the more flexible polymers that have smaller segmental dissymmetry.

We utilize the parameter S_d for obtaining an expression for a critical stretched overlap concentration beyond which extensional relaxation time values measured for nominally dilute polymer solutions show concentration-dependent scaling. We also show that expression of the critical concentration c^{**}, beyond which the polymer solution behavior can be described using a mean field theory for concentrated solutions, also depends on S_d. We recognize that a deeper understanding of extensional rheology response of entangled concentrated solutions (or melts) requires careful determination of how orientation and stretching influence the force-extension curve, tube diameter, number of entanglement stands per volume, interchain and intrachain interactions, among others, as discussed in many insightful recent papers.[12,109,112−116] However, we expect that segmental dissymmetry shall appear as an important parameter in subsequent advances in conceptual and theoretical understanding of extensional rheology response.

We show that the absence of a coil-stretch transition and, consequently, the lack of a rapid transition to the elastocapillary pinching regime do not preclude the existence of an exponential elastocapillary regime for HEC solutions. However, even though the shear viscosity values are higher for the HEC solutions at matched, nondilute concentrations, the absolute values of extensional viscosity of HEC solutions are far below the values obtained for PEO solutions, showing the dramatic influence of lower flexibility and extensibility of polymer chains. Consequently, the addition of a small amount of high-molecular-weight flexible polymer like PEO as an additive increases the spinnability of polymer and protein solutions.[117−119] DoS rheometry measurements for polyelectrolyte solutions[24] show that sodium polystyrene sulfonate (NaPSS) solutions also exhibit $\Delta t_{EC} \ll t_f$ and a small elastocapillary tail, whereas poly(acrylic acid) or PAA solutions show both a pronounced transition from the IC/VC-EC regime and filament lifespan contributed by Δt_{EC}. Likewise, we

https://dx.doi.org/10.1021/acs.macromol.0c00076
Macromolecules 2020, 53, 4821−4835

recently showed that the pinching dynamics of a charged polysaccharide, cellulose gum, mirror the behavior observed for the HEC solutions: $\Delta t_{EC} \ll t_f$, lack of clear IC/VC-EC transition, and a viscoelastic response in the last stage before the pinch-off event.[25] We posit that the constitutive models that explicitly include conformation-dependent drag, finite extensibility, and the physics of coil-stretch transition (and hysteresis) could prove beneficial for capturing the non-monotonic behavior of the extensional rate displayed by the PEO solutions in response to progressively increasing capillarity-induced stress. However, for the unentangled HEC solutions, the shear relaxation time values estimated using the theory of polymer dynamics as well as using fits to the steady shear viscosity data are comparable to the values of λ_E extracted from the relatively short-lived elastocapillary regime. We surmise that the capillarity-driven pinching for HEC solutions is more amenable to analysis by constitutive models based on a single relaxation time ($\lambda_E = \lambda_s$) as long as the finite extensibility effects are included to capture the underlying macromolecular physics.

We anticipate that the approach outlined in this paper can be utilized for polyelectrolyte solutions as well, although additional consideration for electrostatic interactions comes into play, and these will be the focus of a separate paper. We deduce and demonstrate the connection between the semi-flexibility, chain extensibility, extensional rheology response, and pinch-off dynamics that will prove to be immensely useful to chemists, physicists, formulation scientists, and engineers alike. We anticipate that our data and analysis will help in further development of new constitutive models and deeper understanding of how chemical structure and solvent−polymer interactions, as imbibed into three macromolecular properties (flexibility, extensibility, and segmental dissymmetry) affect the static and dynamic properties of polymers in solution.

■ ASSOCIATED CONTENT

Supporting Information

The Supporting Information is available free of charge at https://pubs.acs.org/doi/10.1021/acs.macromol.0c00076.

Image analysis protocol with MATLAB code (PDF)

DoS video obtained at 8000 fps (AVI)

■ AUTHOR INFORMATION

Corresponding Author

Vivek Sharma − *Department of Chemical Engineering, University of Illinois at Chicago, Chicago, Illinois 60608, United States;* orcid.org/0000-0003-1152-1285; Email: viveks@uic.edu

Author

Jelena Dinic − *Department of Chemical Engineering, University of Illinois at Chicago, Chicago, Illinois 60608, United States*

Complete contact information is available at: https://pubs.acs.org/10.1021/acs.macromol.0c00076

Notes

The authors declare no competing financial interest.

■ ACKNOWLEDGMENTS

V.S. would like to acknowledge the funding support by the College of Engineering and the Department of Chemical Engineering at the University of Illinois at Chicago. J.D. was supported by the start-up funds as well as funding by the Campus Research Board (CRB) and also wishes to acknowledge Teaching Assistantship by the Department of Chemistry at UIC. J.D. is currently affiliated with Argonne National Laboratory and Pritzker School of Molecular Engineering at the University of Chicago as a postdoctoral researcher supervised by Prof. Matt Tirrell. J.D. and V.S. acknowledge Alexandro Estrada, who carried out some of the complementary experiments with the HEC solutions as an undergraduate summer researcher. V.S. and J.D. acknowledge Dr. Amanda Marciel (Rice University), Dr. Samanvaya Srivastava (UCLA), Dr. Naveen Reddy (U. Hasselt), Dr. Cynthia Jameson (UIC), and students from the ODES-lab, especially Carina Martinez and Fahed Albreiki, for a close reading of the manuscript.

■ REFERENCES

(1) Rubinstein, M.; Colby, R. H. *Polymer Physics*; Oxford Univ. Press: New York: 2003.

(2) Doi, M.; Edwards, S. F. *The Theory of Polymer Dynamics*; Oxford University Press: New York, 1986; p 406.

(3) de Gennes, P.-G., *Scaling Concepts in Polymer Physics*; Cornell University Press: Ithaca, 1979.

(4) Muthukumar, M. 50th Anniversary Perspective: A perspective on polyelectrolyte solutions. *Macromolecules* **2017**, *50*, 9528−9560.

(5) Wang, Z.-G. 50th anniversary perspective: polymer conformation—A pedagogical review. *Macromolecules* **2017**, *50*, 9073−9114.

(6) Prakash, J. R. Universal dynamics of dilute and semidilute solutions of flexible linear polymers. *Curr. Opin. Colloid Interface Sci.* **2019**, *43*, 63−79.

(7) Schroeder, C. M. Single polymer dynamics for molecular rheology. *J. Rheol.* **2018**, *62*, 371−403.

(8) Shaqfeh, E. S. G. The dynamics of single-molecule DNA in flow. *J. Non-Newtonian Fluid Mech.* **2005**, *130*, 1−28.

(9) Larson, R. G. The rheology of dilute solutions of flexible polymers: Progress and problems. *J. Rheol.* **2005**, *49*, 1−70.

(10) Prabhakar, R.; Gadkari, S.; Gopesh, T.; Shaw, M. J. Influence of stretching induced self-concentration and self-dilution on coil-stretch hysteresis and capillary thinning of unentangled polymer solutions. *J. Rheol.* **2016**, *60*, 345−366.

(11) Prabhakar, R.; Sasmal, C.; Nguyen, D. A.; Sridhar, T.; Prakash, J. R. Effect of stretching-induced changes in hydrodynamic screening on coil-stretch hysteresis of unentangled polymer solutions. *Phys. Rev. Fluids* **2017**, *2*, No. 011301.

(12) Yaoita, T.; Isaki, T.; Masubuchi, Y.; Watanabe, H.; Ianniruberto, G.; Marrucci, G. Primitive chain network simulation of elongational flows of entangled linear chains: stretch/orientation-induced reduction of monomeric friction. *Macromolecules* **2012**, *45*, 2773−2782.

(13) Nguyen, T. Q.; Kausch, H. H. *Flexible Polymer Chains in Elongational Flow: Theory and Experiment*; Springer-Verlag: Berlin, 1999.

(14) Sridhar, T. An overview of the project M1. *J. Non-Newtonian Fluid Mech.* **1990**, *35*, 85−92.

(15) James, D. F.; Walters, K. A critical appraisal of available methods for the measurement of extensional properties of mobile systems. In *Techniques of Rheological Measurement*; Collyer, A. A., Ed.; Elsevier: New York, 1994; pp 33−53.

(16) Sharma, V.; Haward, S. J.; Serdy, J.; Keshavarz, B.; Soderlund, A.; Threlfall-Holmes, P.; McKinley, G. H. The rheology of aqueous solutions of Ethyl Hydroxy-Ethyl Cellulose (EHEC) and its hydrophobically modified Analogue (hmEHEC): Extensional flow response in capillary break-up, jetting (ROJER) and in a cross-slot extensional rheometer. *Soft Matter* **2015**, *11*, 3251−3270.

(17) McKinley, G. H. Visco-elasto-capillary thinning and break-up of complex fluids. *Rheol. Rev.* **2005**, 1−48.

(18) Rodd, L. E.; Scott, T. P.; Cooper-White, J. J.; McKinley, G. H. Capillary break-up rheometry of low-viscosity elastic fluids. *Appl. Rheol.* **2005**, *15*, 12−27.
(19) Petrie, C. J. S. One hundred years of extensional flow. *J. Non-Newtonian Fluid Mech.* **2006**, *137*, 1−14.
(20) Dinic, J.; Biagioli, M.; Sharma, V. Pinch−off dynamics and extensional relaxation times of intrinsically semi−dilute polymer solutions characterized by dripping−onto−substrate rheometry. *J. Polym. Sci., Part B: Polym. Phys.* **2017**, *55*, 1692−1704.
(21) Dinic, J.; Jimenez, L. N.; Sharma, V. Pinch-off dynamics and dripping-onto-substrate (DoS) rheometry of complex fluids. *Lab Chip* **2017**, *17*, 460−473.
(22) Dinic, J.; Sharma, V. Macromolecular relaxation, strain, and extensibility determine elastocapillary thinning and extensional viscosity of polymer solutions. *Proc. Natl. Acad. Sci. U. S. A.* **2019**, *116*, 8766−8774.
(23) Dinic, J.; Zhang, Y.; Jimenez, L. N.; Sharma, V. Extensional relaxation times of dilute, aqueous polymer solutions. *ACS Macro Lett.* **2015**, *4*, 804−808.
(24) Jimenez, L. N.; Dinic, J.; Parsi, N.; Sharma, V. Extensional relaxation time, pinch-off dynamics and printability of semi-dilute polyelectrolyte solutions. *Macromolecules* **2018**, *51*, 5191−5208.
(25) Jimenez, L. N.; Martïnez Narváez, C. D. V.; Sharma, V. Capillary breakup and extensional rheology response of food thickener cellulose gum (NaCMC) in salt-free and excess salt solutions. *Phys. Fluids* **2020**, *32*, No. 012113.
(26) Dinic, J.; Sharma, V. Power laws dominate shear and extensional rheology response and capillarity-driven pinching dynamics of entangled hydroxyethyl cellulose (HEC) solutions. *Macromolecules* **2020**, *53*, 3424.
(27) Latinwo, F.; Schroeder, C. M. Model systems for single molecule polymer dynamics. *Soft Matter* **2011**, *7*, 7907−7913.
(28) Tree, D. R.; Muralidhar, A.; Doyle, P. S.; Dorfman, K. D. Is DNA a good model polymer? *Macromolecules* **2013**, *46*, 8369−8382.
(29) Flory, P. J. Statistical thermodynamics of semi-flexible chain molecules. *Proc. R. Soc. London, Ser. A* **1956**, *234*, 60−73.
(30) Broedersz, C. P.; MacKintosh, F. C. Modeling semiflexible polymer networks. *Rev. Mod. Phys.* **2014**, *86*, 995.
(31) Odijk, T. The statistics and dynamics of confined or entangled stiff polymers. *Macromolecules* **1983**, *16*, 1340−1344.
(32) Morse, D. C. Viscoelasticity of concentrated isotropic solutions of semiflexible polymers. 1. Model and stress tensor. *Macromolecules* **1998**, *31*, 7030−7043.
(33) Frey, E.; Kroy, K.; Wilhelm, J. Viscoelasticity of biopolymer networks and statistical mechanics of semiflexible polymers. In *Advances in Structural Biology*; Elsevier: 1999; Vol. *5*, pp 135−168, DOI: 10.1016/S1064-6000(98)80010-0.
(34) Krishna Reddy, N.; Zhang, Z.; Paul Lettinga, M.; Dhont, J. K. G.; Vermant, J. Probing structure in colloidal gels of thermoreversible rodlike virus particles: Rheology and scattering. *J. Rheol.* **2012**, *56*, 1153−1174.
(35) Lang, C.; Hendricks, J.; Zhang, Z.; Reddy, N. K.; Rothstein, J. P.; Lettinga, M. P.; Vermant, J.; Clasen, C. Effects of particle stiffness on the extensional rheology of model rod-like nanoparticle suspensions. *Soft Matter* **2019**, *15*, 833−841.
(36) Entov, V. M.; Hinch, E. J. Effect of a spectrum of relaxation times on the capillary thinning of a filament of elastic liquid. *J. Non-Newtonian Fluid Mech.* **1997**, *72*, 31−53.
(37) Stelter, M.; Brenn, G.; Yarin, A. L.; Singh, R. P.; Durst, F. Validation and application of a novel elongational device for polymer solutions. *J. Rheol.* **2000**, *44*, 595−616.
(38) Stelter, M.; Brenn, G.; Yarin, A. L.; Singh, R. P.; Durst, F. Investigation of the elongational behavior of polymer solutions by means of an elongational rheometer. *J. Rheol.* **2002**, *46*, 507−527.
(39) Clasen, C.; Plog, J. P.; Kulicke, W. M.; Owens, M.; Macosko, C.; Scriven, L. E.; Verani, M.; McKinley, G. H. How dilute are dilute solutions in extensional flows? *J. Rheol.* **2006**, *50*, 849−881.
(40) Wagner, C.; Bourouiba, L.; McKinley, G. H. An analytic solution for capillary thinning and breakup of FENE-P fluids. *J. Non-Newtonian Fluid Mech.* **2015**, *218*, 53−61.
(41) Zhou, J.; Doi, M. Dynamics of viscoelastic filaments based on Onsager principle. *Phys. Rev. Fluids* **2018**, *3*, No. 084004.
(42) Fontelos, M. A.; Li, J. On the evolution and rupture of filaments in Giesekus and FENE models. *J. Non-Newtonian Fluid Mech.* **2004**, *118*, 1−16.
(43) Bazilevsky, A. V.; Entov, V. M.; Rozhkov, A. N. Liquid filament microrheometer and some of its applications. In *Third European Rheology Conference and Golden Jubilee Meeting of the British Society of Rheology, Edinburgh, UK, 1990*; Elsevier: Edinburgh, UK, 1990; pp 41−43.
(44) Bazilevsky, A. V.; Entov, V. M.; Rozhkov, A. N. Breakup of a liquid bridge as a method of rheological testing of biological fluids. *Fluid Dyn* **2011**, *46*, 613−622.
(45) Bazilevskii, A. V.; Entov, V. M.; Rozhkov, A. N. Breakup of an Oldroyd liquid bridge as a method for testing the rheological properties of polymer solutions. *Polym. Sci., Ser. A* **2001**, *43*, 716−726.
(46) Anna, S. L.; McKinley, G. H. Elasto-capillary thinning and breakup of model elastic liquids. *J. Rheol.* **2001**, *45*, 115−138.
(47) Campo-Deaño, L.; Clasen, C. The slow retraction method (SRM) for the determination of ultra-short relaxation times in capillary breakup extensional rheometry experiments. *J. Non-Newtonian Fluid Mech.* **2010**, *165*, 1688−1699.
(48) Vadillo, D. C.; Mathues, W.; Clasen, C. Microsecond relaxation processes in shear and extensional flows of weakly elastic polymer solutions. *Rheol. Acta* **2012**, *51*, 755−769.
(49) Arnolds, O.; Buggisch, H.; Sachsenheimer, D.; Willenbacher, N. Capillary breakup extensional rheometry (CaBER) on semi-dilute and concentrated polyethyleneoxide (PEO) solutions. *Rheol. Acta* **2010**, *49*, 1207−1217.
(50) Clasen, C. Capillary breakup extensional rheometry of semi-dilute polymer solutions. *Korea-Australia Rheol. J.* **2010**, *22*, 331−338.
(51) Stoltz, C.; de Pablo, J. J.; Graham, M. D. Concentration dependence of shear and extensional rheology of polymer solutions: Brownian dynamics simulations. *J. Rheol.* **2006**, *50*, 137−167.
(52) Pincus, P. Excluded volume effects and stretched polymer chains. *Macromolecules* **1976**, *9*, 386−388.
(53) Pincus, P. Dynamics of stretched polymer chains. *Macromolecules* **1977**, *10*, 210−213.
(54) Somani, S.; Shaqfeh, E. S. G.; Prakash, J. R. Effect of solvent quality on the coil-stretch transition. *Macromolecules* **2010**, *43*, 10679−10691.
(55) de Gennes, P. G. Coil-stretch transition of dilute flexible polymers under ultrahigh velocity gradients. *J. Chem. Phys.* **1974**, *60*, 5030−5042.
(56) Hinch, E. J. Mechanical models of dilute polymer solutions in strong flows. *Phys. Fluids* **1977**, *20*, S22−S30.
(57) Tanner, R. I. Stresses in dilute solutions of bead−nonlinear−spring macromolecules. III. Friction coefficient varying with dumbbell extension. *Trans. Soc. Rheol.* **1975**, *19*, 557−582.
(58) Fuller, G. G.; Leal, L. G. Flow birefringence of dilute polymer solutions in two-dimensional flows. *Rheol. Acta* **1980**, *19*, 580−600.
(59) Wiest, J. M.; Wedgewood, L. E.; Bird, R. B. On coil−stretch transitions in dilute polymer solutions. *J. Chem. Phys.* **1989**, *90*, 587−594.
(60) Schroeder, C. M.; Babcock, H. P.; Shaqfeh, E. S. G.; Chu, S. Observation of polymer conformation hysteresis in extensional flow. *Science* **2003**, *301*, 1515−1519.
(61) Schroeder, C. M.; Shaqfeh, E. S. G.; Chu, S. Effect of hydrodynamic interactions on DNA dynamics in extensional flow: Simulation and single molecule experiment. *Macromolecules* **2004**, *37*, 9242−9256.
(62) Hsieh, C. C.; Larson, R. G. Modeling hydrodynamic interaction in Brownian dynamics: Simulations of extensional and shear flows of dilute solutions of high molecular weight polystyrene. *J. Rheol.* **2004**, *48*, 995−1021.

https://dx.doi.org/10.1021/acs.macromol.0c00076
Macromolecules 2020, 53, 4821−4835

(63) Hsieh, C. C.; Larson, R. G. Prediction of coil-stretch hysteresis for dilute polystyrene molecules in extensional flow. *J. Rheol.* **2005**, *49*, 1081−1089.
(64) Hsieh, C. C.; Li, L.; Larson, R. G. Modeling hydrodynamic interaction in Brownian dynamics: simulations of extensional flows of dilute solutions of DNA and polystyrene. *J. Non-Newtonian Fluid Mech.* **2003**, *113*, 147−191.
(65) Fetters, L. J.; Lohse, D. J.; Richter, D.; Witten, T. A.; Zirkel, A. Connection between polymer molecular weight, density, chain dimensions, and melt viscoelastic properties. *Macromolecules* **1994**, *27*, 4639−4647.
(66) Fetters, L. J.; Lohse, D. J.; Milner, S. T.; Graessley, W. W. Packing length influence in linear polymer melts on the entanglement, critical, and reptation molecular weights. *Macromolecules* **1999**, *32*, 6847−6851.
(67) Fetters, L. J.; Lohse, D. J.; Colby, R. H. Chain dimensions and entanglement spacings. In *Physical Properties of Polymers Handbook*; Springer: 2007; pp 447−454.
(68) Unidad, H. J.; Goad, M. A.; Bras, A. R.; Zamponi, M.; Faust, R.; Allgaier, J.; Pyckhout-Hintzen, W.; Wischnewski, A.; Richter, D.; Fetters, L. J. Consequences of Increasing Packing Length on the Dynamics of Polymer Melts. *Macromolecules* **2015**, *48*, 6638−6645.
(69) Witten, T. A.; Milner, S. T.; Wang, Z. G. Theory of stress distribution in block copolymer microdomains. In *Multiphase Macromolecular Systems*; Culbertson, B. M., Ed.; Plenum: New York, 1989.
(70) Odell, J. A.; Keller, A.; Rabin, Y. Flow−induced scission of isolated macromolecules. *J. Chem. Phys.* **1988**, *88*, 4022−4028.
(71) Odell, J. A.; Muller, A. J.; Narh, K. A.; Keller, A. Degradation of polymer solutions in extensional flows. *Macromolecules* **1990**, *23*, 3092−3103.
(72) Odell, J. A.; Keller, A. Flow-induced chain fracture of isolated linear macromolecules in solution. *J. Polym. Sci., Part B: Polym. Phys.* **1986**, *24*, 1889−1916.
(73) Walter, A. V.; Jimenez, L. N.; Dinic, J.; Sharma, V.; Erk, K. A. Effect of salt valency and concentration on shear and extensional rheology of aqueous polyelectrolyte solutions for enhanced oil recovery. *Rheol. Acta* **2019**, *58*, 145−157.
(74) Hsiao, K. W.; Dinic, J.; Ren, Y.; Sharma, V.; Schroeder, C. M. Passive non-linear microrheology for determining extensional viscosity. *Phys. Fluids* **2017**, *29*, 121603.
(75) Marshall, K. A.; Liedtke, A. M.; Todt, A. H.; Walker, T. W. Extensional rheometry with a handheld mobile device. *Exp. Fluids* **2017**, *58*, 69.
(76) Suteria, N. S.; Gupta, S.; Potineni, R.; Baier, S. K.; Vanapalli, S. A. eCapillary: a disposable microfluidic extensional viscometer for weakly elastic polymeric fluids. *Rheol. Acta* **2019**, *58*, 403−417.
(77) Marshall, K. A.; Walker, T. W. Investigating the dynamics of droplet breakup in a microfluidic cross-slot device for characterizing the extensional properties of weakly-viscoelastic fluids. *Rheol. Acta* **2019**, *58*, 573−590.
(78) Pack, M. Y.; Yang, A.; Perazzo, A.; Qin, B.; Stone, H. A. Role of extensional rheology on droplet bouncing. *Phys. Rev. Fluids* **2019**, *4*, 123603.
(79) Rosello, M.; Sur, S.; Barbet, B.; Rothstein, J. P. Dripping-onto-substrate capillary breakup extensional rheometry of low-viscosity printing inks. *J. Non-Newtonian Fluid Mech.* **2019**, *266*, 160−170.
(80) Zhang, Y.; Muller, S. J. Unsteady sedimentation of a sphere in wormlike micellar fluids. *Phys. Rev. Fluids* **2018**, *3*, 043301.
(81) Wu, S.; Mohammadigoushki, H. Sphere sedimentation in wormlike micelles: Effect of micellar relaxation spectrum and gradients in micellar extensions. *J. Rheol.* **2018**, *62*, 1061−1069.
(82) Omidvar, R.; Wu, S.; Mohammadigoushki, H. Detecting wormlike micellar microstructure using extensional rheology. *J. Rheol.* **2019**, *63*, 33−44.
(83) Schneider, C. A.; Rasband, W. S.; Eliceiri, K. W. NIH Image to ImageJ: 25 years of image analysis. *Nat. Methods* **2012**, *9*, 671−675.
(84) Del Giudice, F.; Tassieri, M.; Oelschlaeger, C.; Shen, A. Q. When Microrheology, Bulk Rheology, and Microfluidics Meet: Broadband Rheology of Hydroxyethyl Cellulose Water Solutions. *Macromolecules* **2017**, *50*, 2951−2963.
(85) Chen, Y.-J.; Steen, P. H. Dynamics of inviscid capillary breakup: collapse and pinchoff of a film bridge. *J. Fluid Mech.* **1997**, *341*, 245−267.
(86) Day, R. F.; Hinch, E. J.; Lister, J. R. Self-similar capillary pinchoff of an inviscid fluid. *Phys. Rev. Lett.* **1998**, *80*, 704−707.
(87) Eggers, J. Nonlinear dynamics and breakup of free-surface flows. *Rev. Mod. Phys.* **1997**, *69*, 865−930.
(88) Eggers, J.; Fontelos, M. A. *Singularities: Formation, Structure, and Propagation;* Cambridge University Press: Cambridge, UK, 2015; Vol. *53*.
(89) Dinic, J.; Sharma, V. Computational analysis of self-similar capillary-driven thinning and pinch-off dynamics during dripping using the volume-of-fluid method. *Phys. Fluids* **2019**, *31*, No. 021211.
(90) Tirtaatmadja, V.; McKinley, G. H.; Cooper-White, J. J. Drop formation and breakup of low viscosity elastic fluids: Effects of molecular weight and concentration. *Phys. Fluids* **2006**, *18*, No. 043101.
(91) Odijk, T. Unfolding kinetics of a wormlike chain under elongational flow. *Polymer* **2017**, *9*, 190.
(92) Radhakrishnan, R.; Underhill, P. T. Impact of solvent quality on the hysteresis in the coil−stretch transition of flexible polymers in good solvents. *Macromolecules* **2012**, *46*, 548−554.
(93) Ryskin, G. Calculation of the effect of polymer additive in a converging flow. *J. Fluid Mech.* **1987**, *178*, 423−440.
(94) Sridhar, T.; Nguyen, D. A.; Prabhakar, R.; Prakash, J. R. Rheological observation of glassy dynamics of dilute polymer solutions near the coil-stretch transition in elongational flows. *Phys. Rev. Lett.* **2007**, *98*, 167801.
(95) Ardekani, A. M.; Sharma, V.; McKinley, G. H. Dynamics of bead formation, filament thinning and breakup in weakly viscoelastic jets. *J. Fluid Mech.* **2010**, *665*, 46−56.
(96) Mathues, W.; Shahid, T.; Hendricks, J.; Clasen, C. An analytical solution for the initial polymer stretch evolution in thinning viscoelastic filaments. *Rheol. Bull.* **2016**, *57*, 57−62.
(97) Amarouchene, Y.; Bonn, D.; Meunier, J.; Kellay, H. Inhibition of the finite-time singularity during droplet fission of a polymeric fluid. *Phys. Rev. Lett.* **2001**, *86*, 3558−3561.
(98) Sharma, V.; Ardekani, A. M.; McKinley, G. H. 'Beads on a String'Structures and Extensional Rheometry using Jet Break-up. In *5th Pacific Rim Conference on Rheology (PRCR-5)*; Sapporo, Japan; Australian Society of Rheology: 2010.
(99) Liang, R. F.; Mackley, M. R. Rheological characterization of the time and strain dependence for polyisobutylene solutions. *J. Non-Newtonian Fluid Mech.* **1994**, *52*, 387−405.
(100) Fuller, G. G.; Cathey, C. A.; Hubbard, B.; Zebrowski, B. E. Extensional viscosity measurements for low−viscosity fluids. *J. Rheol.* **1987**, *31*, 235−249.
(101) Keller, A.; Odell, J. A. The extensibility of macromolecules in solution; a new focus for macromolecular science. *Colloid Polym. Sci.* **1985**, *263*, 181−201.
(102) Celani, A.; Puliafito, A.; Vincenzi, D. Dynamical slowdown of polymers in laminar and random flows. *Phys. Rev. Lett.* **2006**, *97*, 118301.
(103) Wagner, C.; Amarouchene, Y.; Bonn, D.; Eggers, J. Droplet detachment and satellite bead formation in viscoelastic fluids. *Phys. Rev. Lett.* **2005**, *95*, 164504.
(104) Brust, M.; Schaefer, C.; Doerr, R.; Pan, L.; Garcia, M.; Arratia, P. E.; Wagner, C. Rheology of human blood plasma: Viscoelastic versus Newtonian behavior. *Phys. Rev. Lett.* **2013**, *110*, No. 078305.
(105) Haward, S. J.; Sharma, V.; Butts, C. P.; McKinley, G. H.; Rahatekar, S. S. Shear and extensional rheology of cellulose/ionic liquid solutions. *Biomacromolecules* **2012**, *13*, 1688−1699.
(106) Arfin, N.; Bohidar, H. B. Concentration selective hydration and phase states of hydroxyethyl cellulose (HEC) in aqueous solutions. *Int. J. Biol. Macromol.* **2012**, *50*, 759−767.
(107) Larson, R. G. *The Structure and Rheology of Complex Fluids*; Oxford University Press: New York, 1999.

https://dx.doi.org/10.1021/acs.macromol.0c00076
Macromolecules 2020, 53, 4821−4835

(108) Martínez-Richa, A. Determination of molecular size of O-(2-hydroxyethyl) cellulose (HEC) and its relationship to the mechanism of enzymatic hydrolysis by cellulases. *Carbohydr. Polym.* **2012**, *87*, 2129−2136.
(109) Qin, J.; Milner, S. T. Tube diameter of oriented and stretched polymer melts. *Macromolecules* **2013**, *46*, 1659−1672.
(110) Horinaka, J.; Chen, K.; Takigawa, T. Entanglement properties of carboxymethyl cellulose and related polysaccharides. *Rheol. Acta* **2018**, *57*, 51−56.
(111) Horinaka, J.; Yasuda, R.; Takigawa, T. Entanglement Properties of Cellulose and Amylose in an Ionic Liquid. *J. Polym. Sci., Part B: Polym. Phys.* **2011**, *49*, 961−965.
(112) Costanzo, S.; Huang, Q.; Ianniruberto, G.; Marrucci, G.; Hassager, O.; Vlassopoulos, D. Shear and extensional rheology of polystyrene melts and solutions with the same number of entanglements. *Macromolecules* **2016**, *49*, 3925−3935.
(113) Desai, P. S.; Larson, R. G. Constitutive model that shows extension thickening for entangled solutions and extension thinning for melts. *J. Rheol.* **2014**, *58*, 255−279.
(114) Huang, Q.; Hengeller, L.; Alvarez, N. J.; Hassager, O. Bridging the gap between polymer melts and solutions in extensional rheology. *Macromolecules* **2015**, *48*, 4158−4163.
(115) O'Connor, T. C.; Alvarez, N. J.; Robbins, M. O. Relating Chain Conformations to Extensional Stress in Entangled Polymer Melts. *Phys. Rev. Lett.* **2018**, *121*, No. 047801.
(116) Sridhar, T.; Acharya, M.; Nguyen, D. A.; Bhattacharjee, P. K. On the extensional rheology of polymer melts and concentrated solutions. *Macromolecules* **2013**, *47*, 379−386.
(117) Vega-Lugo, A.-C.; Lim, L.-T. Effects of poly (ethylene oxide) and pH on the electrospinning of whey protein isolate. *J. Polym. Sci., Part B: Polym. Phys.* **2012**, *50*, 1188−1197.
(118) Fang, Y.; Dulaney, A. D.; Gadley, J.; Maia, J. M.; Ellison, C. J. Manipulating characteristic timescales and fiber morphology in simultaneous centrifugal spinning and photopolymerization. *Polymer* **2015**, *73*, 42−51.
(119) Fang, Y.; Dulaney, A. R.; Gadley, J.; Maia, J.; Ellison, C. J. A comparative parameter study: Controlling fiber diameter and diameter distribution in centrifugal spinning of photocurable monomers. *Polymer* **2016**, *88*, 102−111.

https://dx.doi.org/10.1021/acs.macromol.0c00076
Macromolecules 2020, 53, 4821−4835